Photo-Curing Behavior and Thermal Properties of Silicone Semi Interpenetrating Polymer Network (Semi-IPN) Organogels

Orkun Kaymakci

Thesis submitted to the faculty of the Virginia Polytechnic Institute and State University in partial fulfillment of the requirements for the degree of

Master of Science
In
Macromolecular Science and Engineering

Robert B. Moore – Committee Chairman
David A. Dillard
Romesh C. Batra

November 27, 2012

Blacksburg, VA

Keywords: organogel, semi-interpenetrating polymer network, photo-curing, modulus, adhesive/cohesive fracture, dynamic mechanical analysis, cold crystallization

Photo-Curing Behavior and Thermal Properties of Silicone

Semi Interpenetrating Polymer Network (Semi-IPN) Organogels

Orkun Kaymakci

ABSTRACT

Silicone hydrogels are receiving considerable interest due to their important biomedical application areas such as contact lenses and wound dressings. The applications of such materials are usually in the hydrated state, as hydrogels. However, manufacturing and molding processes are mostly carried out in the organically solvated state, as organogels. This thesis investigates the effects of some of the manufacturing parameters such as curing time and thermal processing on thermal, mechanical, viscoelastic and adhesive/cohesive fracture properties of silicone semi-interpenetrating polymer network organogels.

Curing time may affect the extent of reaction and the crosslink density of a gel network. In order to investigate the effect of this parameter, materials were photo-cured for different times within the range of 150s to 1800s. Gel content, uniaxial tensile, dynamic mechanical, adhesive fracture and cohesive fracture properties were obtained as a function of photo-curing time and results were correlated with each other in order to have a better understanding of the effects on the material properties. Additionally, thermal properties of the gels were studied in detail. Crystallization and melting behavior of one of the solvents in the organogel were investigated by differential scanning calorimetry and thermal optical microscopy. Correlation between the thermal properties of the solvent and the gel network structure was shown. Dynamic mechanical analysis experiments were performed to investigate the effect of solvent crystallization on the mechanical properties. Finally, the effect of thermal processing parameters such as the heating

rate and the minimum cooling temperatures on the crystallization and the thermo-mechanical properties were studied.

This thesis is dedicated to my first teacher - my mother, Hamidiye Ozberk,

for her continuous love and encouragement.

ACKNOWLEDGMENTS

I would like to express my sincere gratitude and appreciation to my advisor, Dr. Robert B. Moore for his considerable guidance and encouragement throughout the duration of my studies at Virginia Tech. I am also indebted to my advisory committee members, Dr. David Dillard and Dr. Romesh Batra for their time, guidance, and contributions to my studies. I am grateful to this committee for their patience with me as well as for their encouragement over the past two years.

I would also like to thank Dr. Peyton Hopson, Steve Pegram and Kerry Sanders for their collaboration and support to complete this research. They provided me invaluable experience and insights throughout my studies.

I would like to thank Macromolecules and Interfaces Institute (MII), the Institute for Critical Technology and Applied Science (ICTAS) and my sponsor for the opportunities provided me. I also wish to thank Dr. Judy S. Riffle for her help and support.

A special thanks to Geoffrey Tizard for being my mentor and providing motivation when I started to this project. He has always been helpful and encouraging whenever I encountered difficulties with my research.

I especially thank Bikramjit Mukherjee for being my project partner and for valuable discussions about the engineering subjects. Besides being a helpful colleague, he has also been a good friend to me.

I would like to recognize my lab-mates and colleagues including Katie Murray, Dr. Junbo Hou, Dr. Gilles Divoux, Dr. Bruce Orler, Scott Forbey, Mingqiang Zhang, Ninad Dixit, Xijing Yuan, Jeremy Beach, Katherine Finlay, Amanda Neighbors, Elise Naughton, Shantanu Ranade, Nathan

May, Jessica Wright and Ashley Gordon for their assistance and contributions. I always enjoyed working with them.

I am grateful to Sanem Kayandan, for her love and friendship. Words cannot express how thankful I am for her unending support and patience.

My deepest gratitude goes to my family. I would like thank my brother Mustafa Kaymakci, my father Emin Kaymakci and especially my mother Hamidiye Ozberk for their constant love, support and inspiration.

Table of Contents

List of Figures

List of Tables

Chapter 1 : Introduction

Introduction and Motivation

Semi-interpenetrating polymer networks (semi-IPN) consist of one or more crosslinked polymers and one or more linear or branched polymers which do not form a crosslinked system but interpenetrate in the network [1]. Silicone IPN and semi-IPN hydrogels have become increasingly popular due to the combined properties of siloxanes (i.e. high oxygen permeability) and hydrophilic hydrogels (i.e. wettability) [2]. These materials have flexibility similar to natural tissue, high biocompatibility and good transport properties such as high oxygen permeability. Therefore, they have been used in important biomedical application areas such as contact lenses and wound dressing materials.

Synthetic gels can be differentiated based on the type of immobilized constituent. If the immobilized fluid is water, the material is called “hydrogel”. A gel is called “organogel” when the immobilized constituent is a hydrophilic fluid. In general, the fluid is an organic solvent and the specific type of the fluid depends on the application of the organogel. If the gel is filled with nothing but air, the resulting material is called “aerogel” [3]. Most of the studies on synthetic gels have been with either hydrogels or aerogels. However, even though the final applications of these materials are mostly in the hydrated state (such as contact lenses, wound dressings and implants), production and manufacturing of these hydrogels are mostly performed in the organically solvated state (as organogels). Therefore, characterization of the properties of organogels is important, especially from an industrial point of view.

In industry, photo-curing is a widely used technique since it reduces the need for organic solvents and it is faster than thermal polymerization. Photo-curing is often used for free radical

polymerization of acrylate systems[4] and it is also a popular method to prepare silicone IPNs and semi-IPNs[2, 5-10]. Photo-curing time is an important parameter for the manufacturing of these gels and it affects the extent of reaction and the number of crosslinking points of the network. Therefore, it may significantly affect the thermal, bulk mechanical and fracture properties of organogels. Another parameter that may affect the manufacturing process of these gels is the thermal treatment. Besides the tremendous effect of temperature on the viscoelastic properties of organogels, thermal treatment may also cause a change in state (i.e. freezing) of solvents in organogels which may affect the properties significantly. In this thesis, the effect of photo-curing time and thermal processing on various properties of a specific silicone organogel is extensively studied.

Thesis Organization

Chapter 2 of this thesis provides a brief introduction to silicone IPNs and semi IPNs and addresses the specifics of the organogel material studied in this thesis. Experimental details about the material preparation for the bulk and adhesive testing are also discussed in this chapter. Introduction sections of Chapter 3 and Chapter 4 contain detailed literature reviews which discuss studies performed by others as well as in depth background information about the experimental methods used to characterize the organogel.

Chapter 3 mainly discusses the effect of the photo-curing time on the gel network, mechanical, viscoelastic, cohesive fracture and adhesive fracture properties of the organogel. The effect of photo-curing time on the material structure is correlated with the experimental results. In depth comparisons of the changes in different properties are discussed in order to fully understand the effect of photo-curing time.

Chapter 4 mainly focuses on the thermal properties and the effect of thermal phase changes of the solvent on the properties of the gel material. The phase changes in the solvent of the organogel are investigated by DSC, DMA and thermal optical microscopy. Cold crystallization behavior of the solvent is correlated with the characteristics of the gel network. The effect of crystallization and the loss of plasticization on the mechanical properties are discussed. Finally, the effect of processing parameters such as heating rate and minimum cooling temperature on the thermal and mechanical properties are presented.

Chapter 5 summarizes the key findings and conclusions of the experimental results presented in Chapter 3 and 4. Also, possible experiments and suggestions for future work are discussed.

Chapter 2 : Materials and Fabrication of Silicone Organogels

Silicone IPNs and Semi-IPNs

Interpenetrating polymer networks (IPN) are blends of two or more crosslinked networks which are interlaced without covalent bonds between the networks. Semi-IPNs consist of one or more linear or branched polymers which penetrate into one or more crosslinked polymer networks. Figure 2-1 shows the illustration of IPNs and semi-IPNs. In general, IPN and semi-IPN hydrogels have advantageous properties than conventional hydrogels since the desired properties of individual components of the networks can be retained or improved depending on the specific application. Permanent interlacing of the components of IPNs and semi-IPNs can also overcome compatibility issues of the individual components which may limit or control the phase separation[2, 11]. Therefore, these benefits of IPNs have been used to develop silicone hydrogels with high hydrophilicity, good optical properties, high oxygen permeability and desired mechanical properties. Many researchers have studied the synthesis and characterization of silicone IPNs and semi-IPNs composed of silicone macromers and other hydrophilic monomers/macromers [2, 5, 6, 8, 9, 12-18]. Generally, silicone hydrogels combine the high oxygen permeability of silicone and the wettability of hydrophilic polymers, which make them very convenient materials for ophthalmic applications and wound dressings.

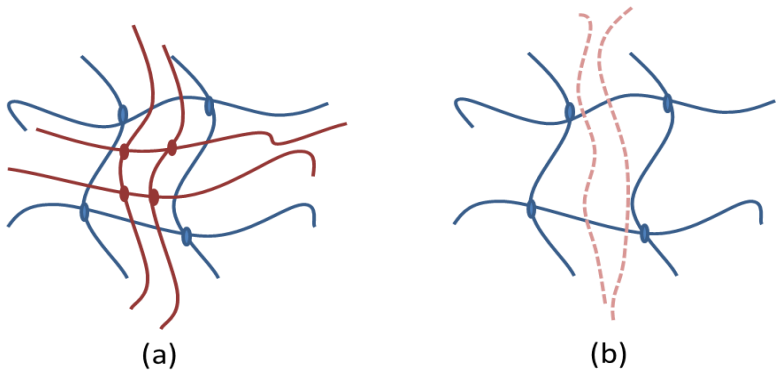

Figure 2-1: IPN composed of two interpenetrating crosslinked network (a) semi-IPN composed of one crosslinked and one interlacing linear polymer (b)

Material and Sample Preparation

Material

The silicone organogel system used in this study was received as a monomer-solvent mixture and it has a solvent content of 45wt%. Two different solvents in the mixture are referred to as Solvent A and B and their contents in the mixture are 25wt% and 20wt%, respectively. Silicone macromer content in the mixture is about 30wt% and the rest of the mixture is composed of hydrophilic monomers and a linear polymer.

Sample Fabrication Process

In order to fabricate the organogels from the monomer-solvent mixture by photo-curing, the mixture was degassed to remove residual oxygen at -85 kPa for at least an hour using a vacuum pump in a vacuum chamber. Then, the vacuum pump was turned off and nitrogen was released into the vacuum chamber. The monomer mixture was immediately put into a nitrogen filled acrylic glovebox. Curing was performed in a nitrogen environment since oxygen gas can interfere with the curing process. The temperature of the glovebox was equilibrated to 60°C using a COY Laboratory Products® heater. The degassed mixture was kept in the heated

glovebox for at least 45 minutes before curing to make sure the temperature of the mixture was equilibrated at 60°C. During the curing process, all natural light sources were blocked and the overhead fluorescent lighting was turned off. The room was lit by yellow fluorescent lighting (Philips® F32T8/TL 730) which lacks the wavelengths below 490 nm. To cure the monomer mixture, Philips® TLK 40W/03 actinic lights were used as the radiation source, which emit radiation in the range of 380-480 nm. Figure 2-2 shows the organogel curing setup and the acrylic glovebox.

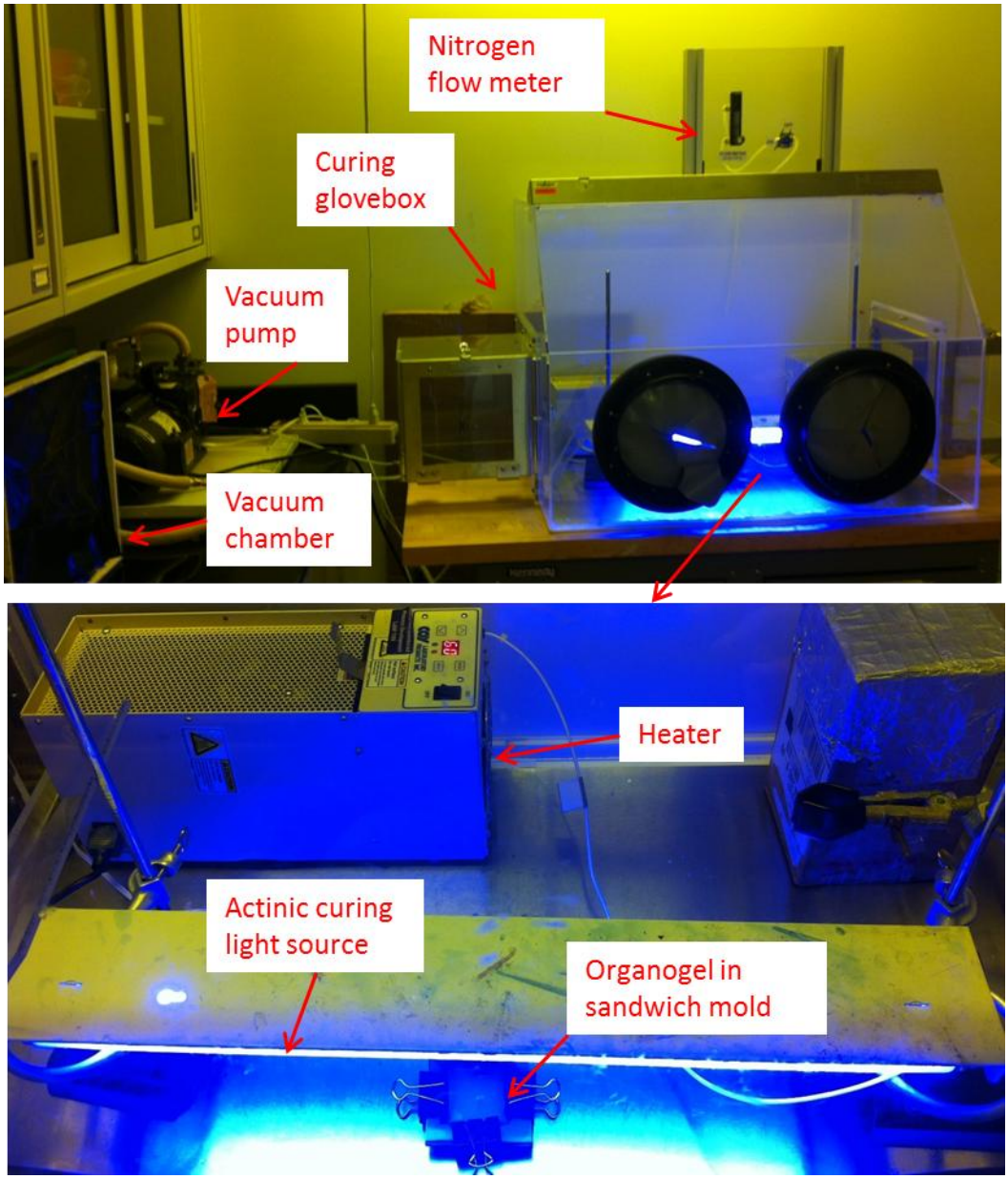

Figure 2-2: Organogel curing setup and acrylic glow box

Bulk Sample Fabrication

In order to prepare bulk samples of the organogel, rectangular polypropylene sheets were used as molds. A rubber silicone window with a thickness of 1.5 mm was placed between two 1.6 mm thick PP molds to set the thickness of the organogel sample. Two rigid acrylate outer walls with

6 mm thickness were placed both on the top and the bottom of the specimen to reduce the thickness variation along the sample (Figure 2-3).

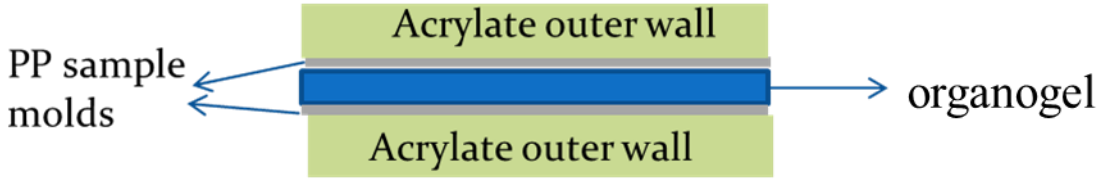

Figure 2-3: Bulk material preparation

After the preparation of 5-layer sandwich mold, binder clips were attached to the sides of the mold to prevent monomer leakage (Figure 2-4). Then, the mold was filled with the monomer-solvent mixture using a plastic pipette. To polymerize the mixture, the filled sandwich mold was placed 10 cm below the actinic lights, where the intensity of the photo-radiation was 0.5 mW/m^2.

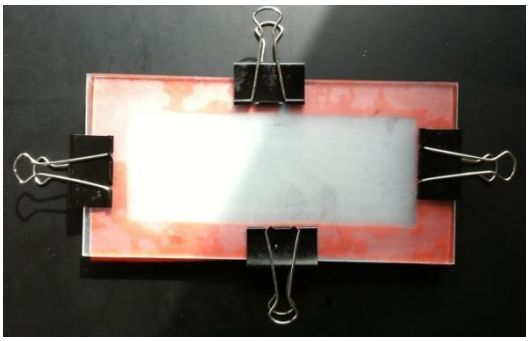

Figure 2-4: Sandwich mold for bulk material preparation

Adhesive Sample Preparation

To characterize the adhesive properties of the organogel, wedge test specimens were prepared. A rectangular cyclo-olefin polymer was used as a substrate material. The substrate polymer has a glass transition temperature above the curing temperature, very low surface energy, high optical clarity, and low moisture absorption. The modulus of elasticity of the material is 2100 MPa[17]. Prior to curing, the substrates were cleaned with reverse osmosis water and the thickness of each

adherend was measured using a Mitutoyo® micrometer (Model ID-H530E). The average thickness of an adherend specimen was 0.74 mm. Thin films (thickness of 0.12 mm) of polycarbonate (PC) spacers were attached to each end of the substrates using pressure sensitive adhesive (PSA) tape to control the thickness of the organogel layer. Then, a plastic pipette was used to place a small amount of monomer mixture in the space between the substrates and the polycarbonate films and the other substrate was placed slowly on the top of the monomer mixture (Figure 2-5). After the curing, the PSA tape and PC spacers were removed. The thickness of the organogel-adherend system was measured again.

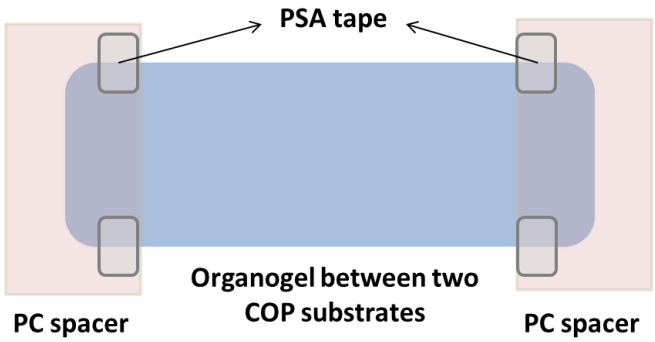

Figure 2-5: Wedge test specimen preparation

Chapter 3 : Effect of Curing Time on Thermal, Viscoelastic, Mechanical and Adhesive/Cohesive Fracture Properties

Introduction

This chapter discusses the effect of photo-curing time on different properties of the organogel material. As stated in Chapter 1, photo-curing time is an important parameter for the manufacturing of photo-cured materials. The crosslink density of a network and the extent of polymerization/crosslinking reactions are affected by the photo-curing time. Therefore, viscoelastic, thermal, mechanical and fracture properties of materials can be greatly affected by the curing time.

During photo-curing, functional monomers and oligomers polymerize into crosslinked polymer networks. Photo-curing can occur by free radical polymerization or cationic polymerization. However, free radical polymerization is mostly used by industry to cure inks, adhesives and coatings. Rapid polymerization rates, low heat generation, low energy requirements and less need for organic solvents are the main advantages of photo-curing. On the other hand, material thickness, fillers, glass transition temperature and outdoor durability of the cured systems are limitations of photo-curing and photo-cured materials[19]. Depending on the absorption range of photo-initiator compounds, different sources such as fluorescent, mercury or Xenon lamps can be used. During the free-radical curing process, photoinitiators absorb the exciting photo radiation and initiator radicals are formed by intramolecular cleavage of the initiators. Then, the free radicals add up with the reactive monomers or oligomers, growing the polymer chain or the crosslinked network[19, 20].

Different studies showed that photo-curing time significantly increases the extent of reaction[21-23], polymerization shrinkage[24] and crosslink density[25] of acrylate based light-cured resin composites. For a relatively weak material such as a silicone hydrogel or organogel, these changes may significantly affect the important material characteristics such as viscoelastic, thermal, mechanical and fracture properties. Therefore, it may be possible to alter the properties of photo-cured materials by changing the curing time.

In general, properties such as modulus, hardness, tensile strength and elasticity of an elastomer depend on the crosslink density of a material. According to the theory of rubber elasticity, the average molecular weight between the crosslinks can be calculated by Equation 3-1[26, 27].

$$\sigma = \frac{\rho.R.T}{M_c}\left(\lambda - \lambda^{-2}\right) \tag{3-1}$$

where σ is the stress, ρ is the density, R is the gas constant, T is the absolute temperature, λ is the extension ratio (strain (ε) +1), and M_c is the average molecular weight between the crosslinks of active chains.

Crosslink density is also an important parameter for the fracture properties of elastomers such as hydrogels. Due to the viscous flow, low molecular weight uncrosslinked polymers fracture at low stresses without any chemical bond breakage. As the crosslink density increases, molecular weight of the network increases so chains cannot flow due to the branched chains. Once the 3-D crosslinked network forms (gel point), breakage of chemical bonds is necessary for fracture to occur. Therefore, to create two fractured surfaces, rupture of chemical bonds will require higher energy, increasing the strength of the material. Viscoelasticity of a network is also a very important parameter influencing the fracture properties and is greatly affected by the crosslink

density of a network. As the crosslink density increases, higher energy will be stored due to the increasing elasticity which may act as a driving force for the fracture. As a result, brittle fracture may occur at low elongations at higher crosslink densities. At lower crosslink densities, viscous component may dissipate some of the input energy as heat, delaying the fracture[28].

Characterization of the properties of silicone hydrogels is a popular research area in industry and academia due to their importance in biomedical applications. Among these studies, dynamic mechanical analysis is a popular method to characterize the viscoelastic, thermal and mechanical properties of these materials. Chauhan et al. investigated the dynamic mechanical properties of silicone hydrogels while the samples were submerged in water. They showed that both storage modulus and loss modulus of hydrogels increase with increasing silicone content. Also, increasing silicone content showed an increase in the frequency dependence of the materials[29]. Abbasi et al. compared the properties of silicone IPNs made of polydimethylsiloxane (PDMS) and polyhydroxyethylmethacrylate (pHEMA) with their physical blends both in dry and hydrated state. The IPNs showed better mechanical properties than their physical blends [15]. Also, DMA analysis of silicone hydrogels showed a phase separation behavior of silicone part and the other network. However, these materials still showed hydrophilic properties which are very important for biomedical applications[15, 16].

Dynamic mechanical analysis basically characterizes viscoelastic and mechanical properties as a function of temperature, frequency and time. A small sinusoidal deformation is applied at a certain frequency and the deformation is controlled either by stress or strain. The two important properties measured by DMA are stiffness and damping. Modulus is used to express the stiffness and tan delta is used to express the damping. In DMA, stress and strain are functions of frequency and time (Equation 3-2).

$$\tau = \tau_0 \sin(\omega t + \delta) \qquad \gamma = \gamma_0 \sin(\omega t) \tag{3-2}$$

where τ and γ are the shear stress and the shear strain respectively, ω is the angular frequency of oscillation, δ is the phase lag between stress and strain, and t is the time. Shear stress can be rewritten as in Equation 3-3 by separating its in-phase and out-of-phase components.

$$\tau = \tau_0 sin(\omega t) cos\,\delta + \tau_0 cos(\omega t) sin\delta \tag{3-3}$$

Shear storage modulus measures the energy stored during elastic shear deformation of a viscoelastic material. Shear loss modulus measures the energy lost as heat during shear deformation and represents the viscous portion of viscoelastic material. Equation 3-3 can be modified to obtain storage and loss modulus.

$$\tau = \gamma_0 G' sin(\omega t) + \gamma_0 G'' cos(\omega t) \tag{3-4}$$

where $G' = \frac{\tau_0}{\gamma_0} cos\,\delta$ is the shear storage modulus and $G'' = \frac{\tau_0}{\gamma_0} sin\,\delta$ is the shear loss modulus. As mentioned above, tan delta measures the damping characteristics of the material. It is basically the ratio of the loss modulus to the storage modulus[30].

$$tan\delta = \frac{G''}{G'} \tag{3-5}$$

Polymers also undergo molecular transitions due to the relaxation of the chains. Glass transition is the onset of long range segmental motions and is generally designated as the α transition. The α transition occurs at the highest temperature and other more localized transitions occur at lower temperatures (β and γ transitions). Maximal values of tanδ are used to determine these type of transitions. Figure 3-1 shows the α, β, and γ transitions and glassy, leathery, and rubbery viscoelastic regions of a thermoset material such as a chemically crosslinked gel[31]. It should

be noted that the viscoelastic properties such as storage modulus and damping are functions of time and temperature. Therefore, viscoelastic properties respond to temperature changes as well as the changes in deformation frequency.

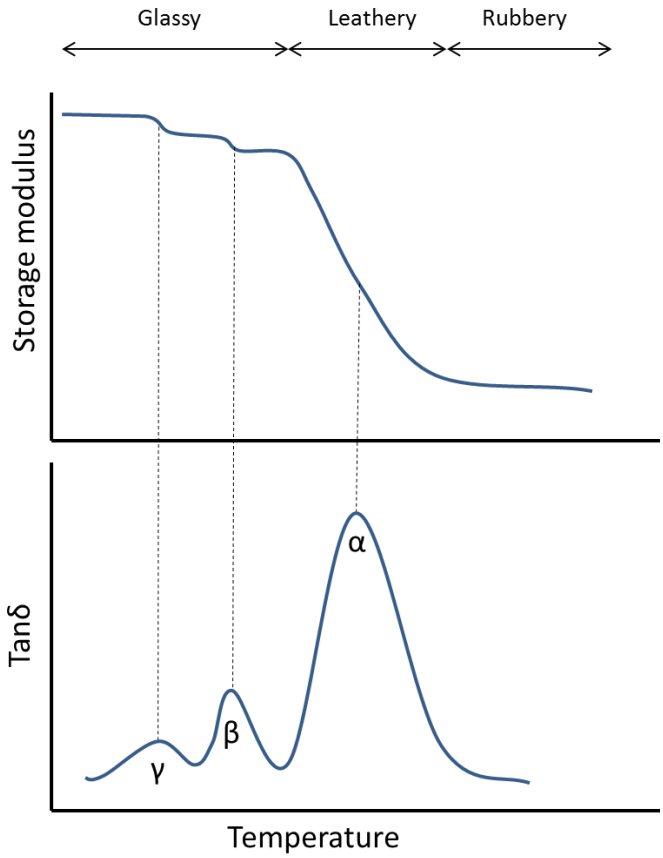

Figure 3-1: Relaxations and viscoelastic regions of a viscoelastic thermoset material

To characterize the tensile properties of soft elastomers such as hydrogels, different mechanical models (Hookean, neo-Hookean and Mooney-Rivlin) have been discussed in the literature. Hookean model fails to characterize the non-linear mechanical behavior of rubber-like soft elastomers due to their non-linear stress-strain response[32]. However, the neo-Hookean model

is widely used to characterize the mechanical properties of hydrogels and rubber-like elastomers [32-35]. In the neo-Hookean model, strain energy function (U) is expressed in Equation 3-6.

$$U = \frac{G}{2}\left(\lambda_x{}^2 + \lambda_y{}^2 + \lambda_z{}^2 - 3\right) \tag{3-6}$$

where λ is the extension ratio ($\mathcal{E}$ + and G is the shear modulus. Since, rubber-like crosslinked elastomers are often assumed to be incompressible (Figure 3-2)[36],

$$\lambda_x \lambda_y \lambda_z = 1 \tag{3-7}$$

Extension ratios in the transverse directions should be equal to each other,

$$\lambda_x = \lambda_y = \lambda_z{}^{-1/2} \tag{3-8}$$

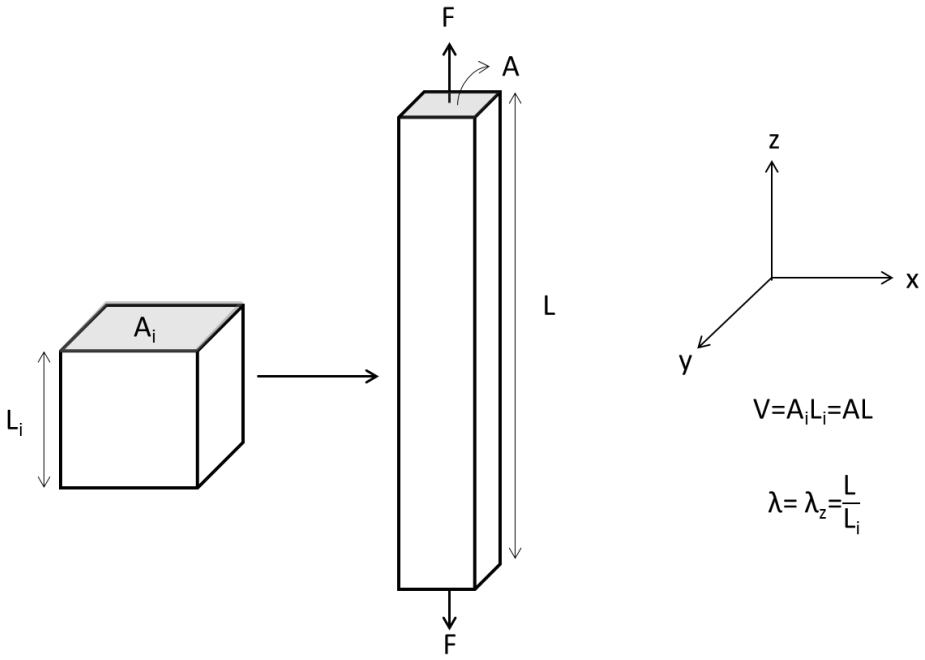

Figure 3-2: Incompressibility of rubber-like elastomers and deformation directions

therefore, Equation 3-6 is modified to

$$U = \frac{G}{2}\left(\lambda^2 + \frac{2}{\lambda} - 3\right) \tag{3-9}$$

where λ is the extension in the longitudinal direction (λ_z).

The derivative of the strain energy function with respect to the extension ratio provides the engineering stress. Using Equation 3-11, shear modulus of the rubber-like elastomers can be determined by the neo-Hookean model. Since Poisson's ratio (ν) of these materials is almost 0.5, elastic modulus can also be calculated using this approach.

$$G = \frac{E}{2(1+\nu)}, \text{ for } \nu = 0.5,\ E = 3G \tag{3-10}$$

$$\frac{dU}{d\lambda} = \sigma = G\left(\lambda - \frac{1}{\lambda^2}\right) = \frac{E}{3}\left(\lambda - \frac{1}{\lambda^2}\right) \tag{3-11}$$

As mentioned in Chapter 1, silicone hydrogels have very important biomedical application areas. These types of materials are usually very soft, however they are also quite brittle, which may create problems both in applications and in manufacturing processes. Therefore, characterization of both cohesive and adhesive fracture properties of these materials is crucial. Cohesive fracture behavior of hydrogels is studied extensively in the literature; however, research on this type of materials in the organically solvated state is very limited. Creton et al. studied the fracture properties of Poly(dimethylacrylamide)/Silica hybrid hydrogels by single edge notch fracture experiments. They calculated the fracture toughness of the materials in mode I by the Rivlin and Thomas[37] energy balance analysis. They showed that the critical energy release rate ($\mathcal{G}_c$) of the hybrid hydrogels significantly increases with the increasing inorganic silica nanoparticle content[38]. Shull et al. investigated the fracture behavior of triblock copolymer gels in mode I.

The strain energy density model used to characterize the fracture properties of the materials reduces to the neo-Hookean model for small strains. However, due to the finite extensibility of the chains, they used a fitting parameter to characterize the fracture at larger strains[33]. The fracture model for the higher strains was initially proposed by Gent for rubber[39].

Tizard studied the cohesive fracture properties of semi-IPN silicone organogels by using constrained tension fracture tests. In his research, fracture characterization of these types of materials were performed over a range of temperatures and rates and fracture master curves were obtained using the "time temperature superposition principle (TTSP)" [18]. In this thesis, the same "constrained tension fracture" experiments are adapted to characterize the effect of curing time on cohesive fracture properties of the silicone organogels. According to the Griffith`s energy criterion[40], when the energy released by the growth of a unit area of crack exceeds the energy to create new surfaces, crack propagation occurs. Therefore, steady-state fracture energy for mode I fracture is calculated by taking the derivative of the strain energy with respect to the area change [18, 41].

$$G_I = \frac{dU}{dA} = U_0 h_0 = \frac{1}{6} E(\lambda_x^{\,2} + \lambda_y^{\,2} + \lambda_z^{\,2} - 3) h_0 \qquad (3\text{-}12)$$

where U is the strain energy density, A is the crack area, h_0 is the initial height and G is the shear modulus of the material. Constrained tension fracture specimen and the deformation directions are shown in Figure 3-3. The initial crack length is shown as a_0.

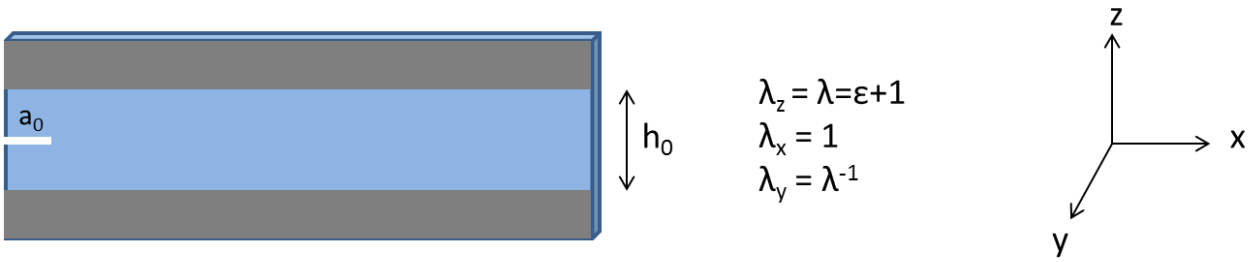

Figure 3-3: Mode I fracture specimen and deformation directions

Higher curing times should cause higher degrees of crosslinking; therefore, materials will behave stiffer. Accordingly, more brittle fracture may occur at higher curing times.

Interfacial fracture or adhesive properties of soft elastomers such as hydrogels or organogels are also very important for the applications of these kinds of materials. For example, many hydrogel products are produced by molding techniques in which the adhesion mechanism between a rigid mold and a cured soft gel is extremely important. Molecular interactions between two interfaces cause the adhesion phenomena and in most cases, adhesion is not quantitatively predictable without destructive test of the interface[42]. Energy release rate ($\mathcal{G}$) (energy required to grow a crack by a unit area) is generally used to characterize the interfacial fracture[42].

During the interfacial fracture of soft elastomers, contribution of the elastically stored energy is crucial. The fracture process involves high strains and the stored elastic energy is dissipated as a result of the fracture[43]. The classical Lake-Thomas theory explains the elastic contribution by correlating the fracture energy to the energy stored in polymer bonds[44].According to this theory, the fracture energy is expressed by:

$$\mathcal{G} = K\sqrt{M_x} \tag{3-13}$$

where K is a constant related with the bond strength and density of a polymer, M_x is the mean molecular weight between the crosslinks[45]. Therefore, according to the Lake-Thomas theory, there is a linear relationship between the fracture energy and the square root of the molecular weight between the crosslink points. Thus, as the crosslink density of a soft elastomer increases, fracture strength should decrease. Gent et al. showed that tear strengths are lower for a given tear rate at the higher levels of crosslinking[46].

Since Lake-Thomas theory only considers the elastic contribution, it has an important limitation. The viscous dissipation of energy by the friction of the polymer chains at lower deformation rates away from the crack tip also has an important contribution to the fracture energy since it is an important dissipative factor. Linear viscoelastic theory is generally used to predict the dissipation which occurs away from the crack tip[43].

Adhesion between soft viscoelastic elastomers and rigid surfaces are generally characterized by peel tests and JKR tests [47]. Creton et al. studied the interfacial adhesion between a soft viscoelastic layer acrylic adhesive and a rigid surface using a novel probe method. In this study, a flat rigid probe was brought in contact with a soft elastomer, and then removed at a constant velocity. Before the debonding, the probe was stopped at some level of tensile force and the time required for the complete debonding was analyzed[47].

Murray studied the interfacial fracture properties of semi-IPN silicone organogel materials. Organogels were cured between two relatively rigid thermoplastic polymers and fracture experiments were performed at different temperatures. Basically, a wedge was inserted between two adherends bonded by organogel materials and crack propagation rates were calculated. Then, the strain energy release rate vs. crack propagation plots were shifted using the TTSP theory to

obtain master curves[17]. In this thesis, to study the effect of curing time on the interfacial fracture properties, the same wedge test experimental procedure was used. The wedge test is a very similar method to the double cantilever beam test which is a widely used mode I fracture test. Originally, the wedge test is developed to characterize the durability of aluminum alloys used in aircrafts in different environments[48]. ASTM D 3762 standard describes the Boeing wedge test[49]. Test configuration is shown in Figure 3-4.

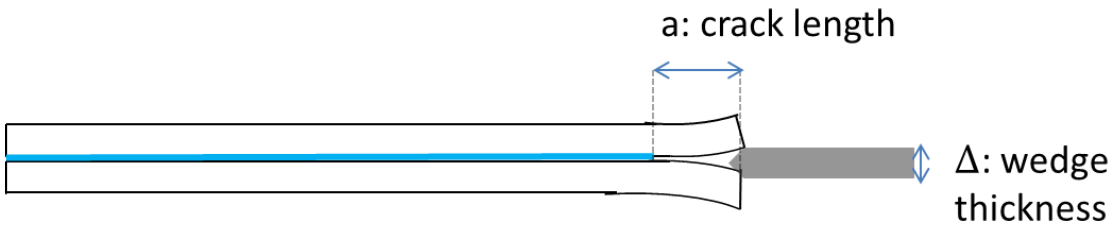

Figure 3-4: Wedge test configuration

Ghatak et al. investigated the measurement of work of adhesion between a soft confined film and a flexible plate[50]. They considered the energy of adhesion between the soft elastic film and the flexible adherend, the energy required to bend the adherend and the elastic energy of the adhesive to calculate the fracture energy. They also assumed that the soft elastic film perfectly adheres to the adherend[17, 50]. The strain energy release rate equation for this model is shown in Equation 3-14.

$$\mathcal{G} = \frac{9D(\Delta - h)^2}{2a^4} g(ak) \tag{3-14}$$

where D represents the flexural rigidity of the adherend, Δ is the wedge thickness, a is the crack length, h is the adhesive film thickness and, $g(ak)$ is the correction factor.

The flexural rigidity (D) is a measure of the adherend` s resistance to bending. Calculation of the flexural rigidity (Equation 3-15) is important in order to consider the bending energy of the adherend for the strain energy release rate calculations.

$$D = \frac{Et^3}{12(1-\nu^2)} \tag{3-15}$$

where E is the elastic modulus, t is the thickness and ν is the Poisson`s ratio of the adherend.

The correction factor $g(ak)$ is required to implement the geometry of the deformation and the material properties and k^{-1} is the characteristic length scale to measure the relative deformability of the plate and the film[50, 51].

$$k^{-1} = \left[\frac{Dh^3}{96G}\right]^{1/6} \tag{3-16}$$

where G is the shear modulus of the soft film.

Calculation of the correction factor is shown in Equation (3-17).

$$g(ak) = \frac{8(ak)^4\left(12 + 46(ak) + 72(ak)^2 + 56(ak)^3 + 21(ak)^4 + 3(ak)^5\right)}{3\left(6 + 12(ak) + 9(ak)^2 + 2(ak)^3\right)^3} \tag{3-17}$$

The effect of curing time on viscoelastic, thermal, mechanical and cohesive/adhesive fracture properties of semi-IPN silicone organogels can be crucial since curing time significantly affects the extent of reaction and the crosslink density of the materials. This chapter discusses the methods used to characterize these effects and experimental results of the effect of curing time.

Experimental Methods

Solvent Extraction

The effect of the curing time on the gel content of the silicone semi-IPN organogels were characterized by a solvent extraction method. The organogels were cured in sandwich molds as described in Chapter-2. The approximate sample dimension was 12.6 x 6.7 x 1.5 mm. The samples were placed into a boiling extraction solution and kept there for 6 hours, stirring constantly by a magnetic stirrer. Then, the samples were washed with reverse osmosis water and left in a beaker filled with water for overnight in order to remove the residual extraction solvent. Then, the resulting hydrogel samples were put into a vacuum oven at -95 kPa pressure and at 90°C temperature for 24 hours to evaporate water. Finally, the dry samples were weighed.

Uniaxial Tension Test

In order to study the effect of curing time on stiffness and other tensile properties, uniaxial tensile tests were performed. Cured organogel sheet dimension was approximately 12.6 x 6.7 x 1.5 mm. A standard ASTM # D 638-5-IMP punch die was used to punch dog-bone specimens from the bulk organogel sheet. Pressure sensitive adhesive tape was placed at the end of the specimens to reduce the damage from the tester grips. Also, white reflecting tape was placed on the specimens for the laser extensometer measurements as shown in Figure 3-5.

Figure 3-5: Dog-bone specimen for the uniaxial tensile tests

Prior to the uniaxial tensile experiments, thickness of the each specimen was measured using a Mitutoyo® micrometer. For the uniaxial tensile testing of the specimens, an Instron 5848 Microtester equipped with a 50 N load cell (Interface, SMT-50) was used. Samples were secured using pneumatic grips (Instron, 2712-019) and air pressure of the grips was set to 90 kPa. A laser extensometer (Fiedler Optoelektronik GmbH) was placed in front of the test specimen to measure the axial strain accurately. Figure 3-6 shows the Instron Microtester and the laser extensometer. The mounted dog-bone specimen is shown in Figure 3-7.

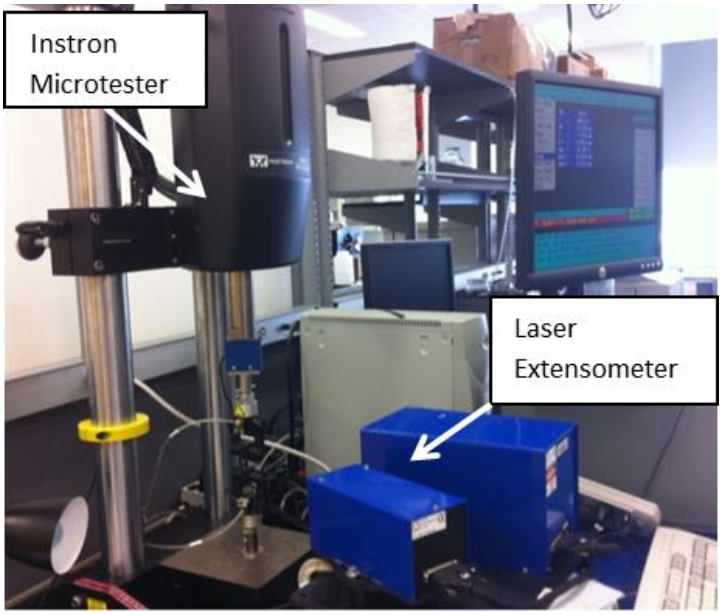

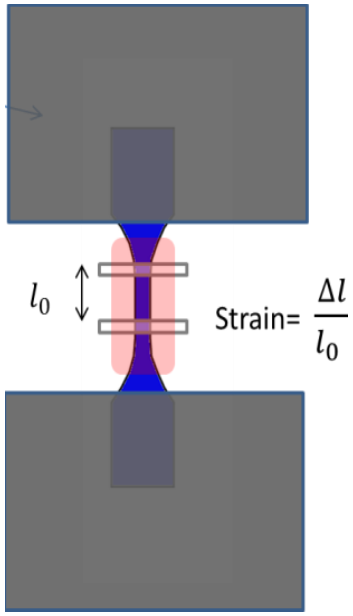

Figure 3-6: Instron Microtester and laser extensometer

Figure 3-7: Mounted dog-bone specimen

The displacement rate was 2 mm/s and all the tests were performed at 22°C. Laser extensometry is a non-contact technique to measure elongations accurately, especially for soft materials with a high strain behavior. To measure strain, laser source of the extensometer emmited laser on the sample (Figure 3-7), and white electrical tape reflected the laser light. Reflected light is detected by the detector. Laser detector records the position of the reflected laser light and axial strain can be measured accurately.

Dynamic Mechanical Analysis

Thermomechanical and viscoelastic properties of the materials were studied by dynamic mechanical analysis in shear mode. TA Instruments DMA Q800 equipped with a liquid nitrogen cooler tank was used to perform the tests. Approximately 10 x 10 x 1.5 mm square samples were cut from a cured sheet of organogel and placed into shear sandwich clamps. Samples were compressed enough to prevent slippage during the tests. Figure 3-8 shows the DMA shear sandwich set up and the shear deformation diagram.

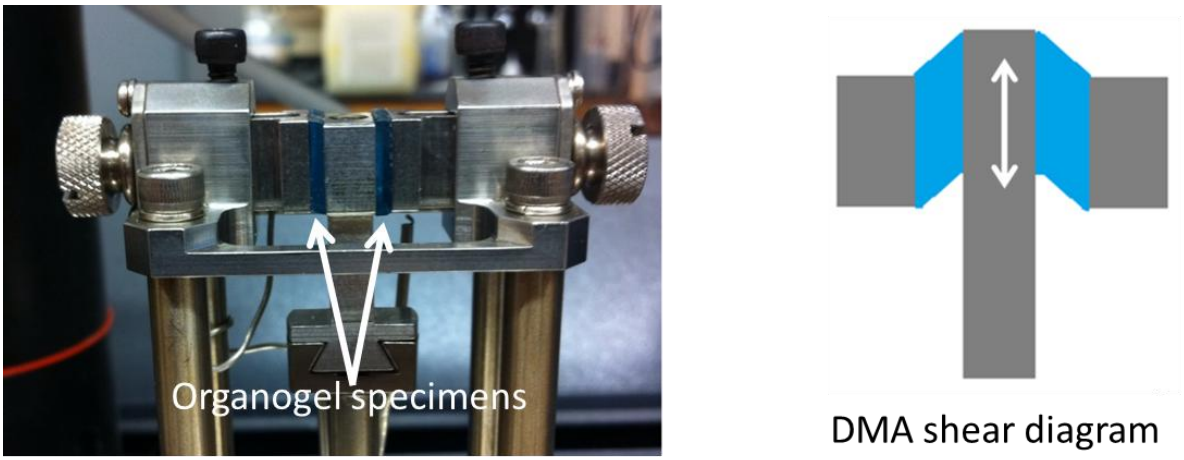

Figure 3-8: DMA shear sandwich set up and the shear diagram

Temperature ramp tests were performed over a temperature range of -120°C to 100°C. The DMA was used in strain controlled mode and the strain amplitude was set to 10μm. Samples were initially equilibrated at -120°C and kept at that temperature for 5 minutes. Then, the temperature was increased to 100°C by 2°C/min increments. A single sinusoidal deformation frequency of 1 Hz was used during the temperature ramp. Shear modulus and tan δ plots were obtained as a function of temperature.

Constrained Fracture and Relaxation Tests

To characterize the effect of photo-curing time on the cohesive fracture properties of the organogel, constrained fracture tests were performed. Organogel sheets with an approximate dimension of 200 x 75 x 1.5 mm were prepared using the procedure in Chapter 2. On the both sides of the gel sheet, 2 mm wide pressure sensitive adhesive (PSA) tape was placed across the specimens to reduce the damage induced from metal grips when mounting and testing the specimen in the load frame (Figure 3-9). The length of the area between the PSA tape was about 25 mm. Aluminum strips were placed on the tape and hole locations were marked. Holes were punched on the organogel accordingly. Then, double sided tape was placed on the aluminum strips (between each hole) and the strips were placed on the organogel sample again (Figure 3-9).

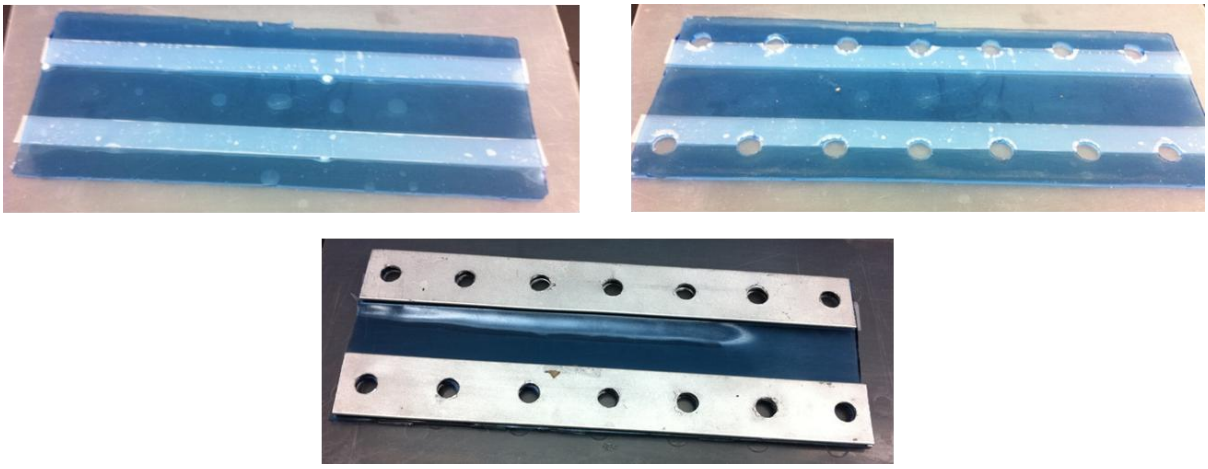

Figure 3-9: Constrained fracture test specimen preparation

After the aluminum bars were placed, the organogel test sample dimension was 200 mm by length and 25 mm by height. The specimen was secured in the pure shear grips and mounted on an Instron 5848 Microtester equipped with an Instron 2 kN load cell.

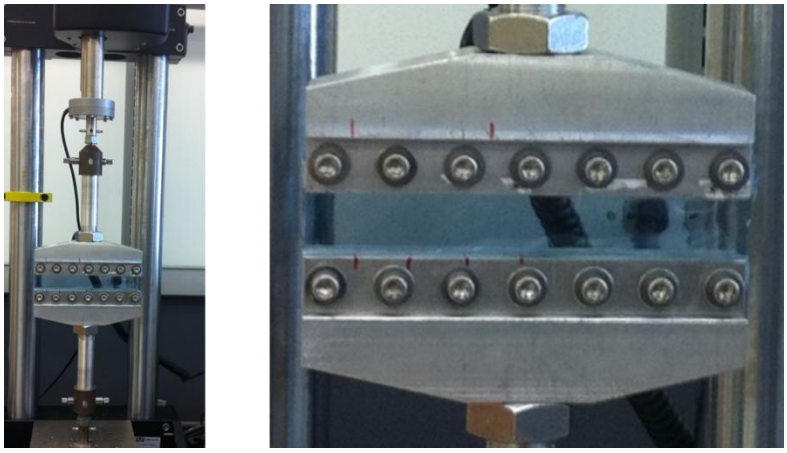

Figure 3-10: Mounted organogel test specimen for the constrained fracture tests

Once the sample mounted on the testing equipment, a 10 mm long initial notch was induced using a razor blade along the midline of the specimen. Then, the pre-cracked samples were strained to 40% of the initial height of the specimen in 1 second and strain level kept constant until the crack propagated across the entire length of the sample. All the tests were performed at 22°C.

During the experiments, the crack propagation was recorded by a Photron high speed camera (APX-RX). Camera resolution was 1024 x 256 and image record rate was 500 frames per seconds (fps). A high speed camera image showing the initial notch is presented in Figure 3-11.

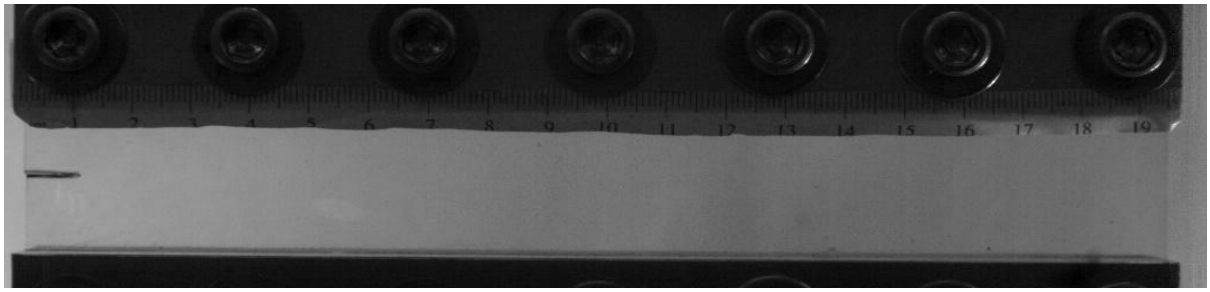

Figure 3-11: Initial notch showing on a high speed camera image

PFV (Photron Fastcam Viever) image processing software was used to process the crack propagation data. Each 100th image was analyzed to calculate the crack length. Since the frame rate was 500 fps, time interval between the each recorded image was 0.2 seconds. To measure the crack length, a straight line was drawn from the crack tip to the attached paper ruler and the crack length was recorded manually (Figure 3-12). Therefore, crack propagation rates were calculated.

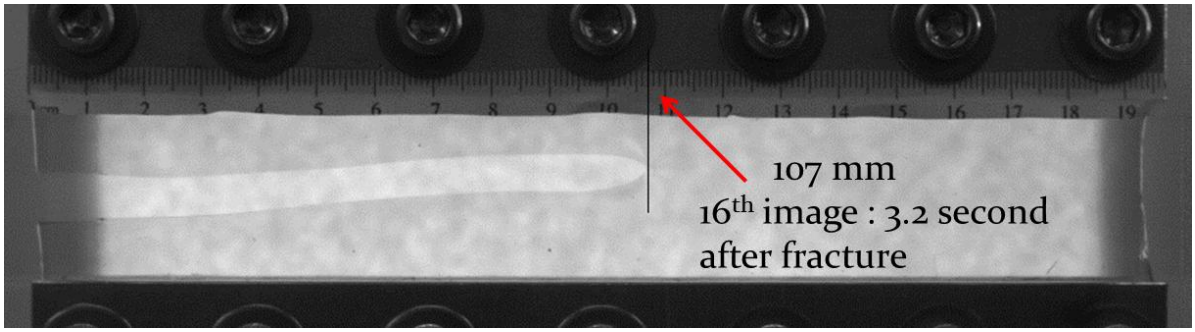

Figure 3-12: Measurement of crack length

Constrain tension relaxation tests were additionally performed in order to implement the time dependent relaxation effects into the cohesive fracture strain energy release rate (SERR) calculations. Organogels without an initial notch were strained using the same strain profile with the fracture tests. The stresses were recorded as a function of time to obtain the effective modulus of the organogels during the applied strain profile. Figure 3-13 shows a strained constrained tension relaxation test specimen.

Figure 3-13: Constrained tension relaxation test specimen

Once the stress relaxation curves were obtained, the effective modulus values were calculated using Equation 3-18[18].

$$E(t) = \frac{\sigma(t)}{\varepsilon} \tag{3-18}$$

Wedge Test

In order to characterize the interfacial fracture properties of the organogels, wedge tests were performed. Details about the wedge test sample fabrication and the curing processes were given in Chapter-2. Figure 2-5 shows the schematic of the wedge test preparation.

A piece of graph paper was attached on the back of the adherend to measure the crack length during the wedge test. A wedge with a thickness of 1.1 mm was inserted to commence the crack propagation. Figure 3-4 shows the wedge test configuration and Figure 3-14 shows the side view of the wedge test.

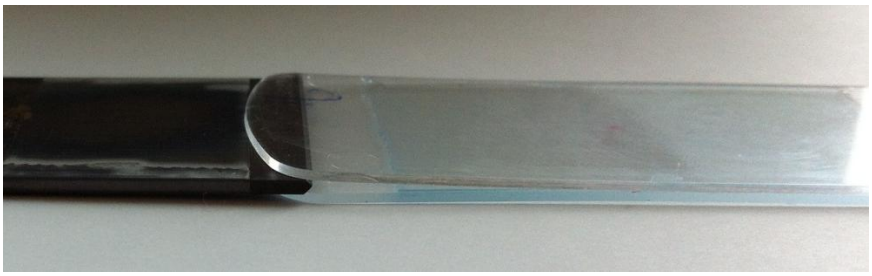

Figure 3-14: Side view of the wedge test

A Photron high speed camera was used to record the test process and crack lengths were measured using the images from the camera. The high speed camera resolution was 1024 x 512 and the frame rate was 60 fps. A wedge test image from the camera is shown in Figure 3-15.

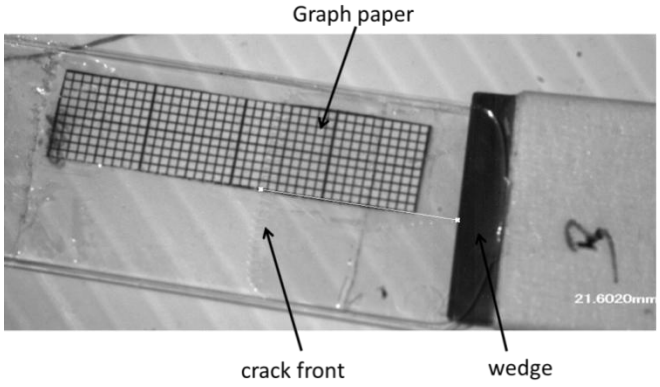

Figure 3-15: Wedge tests high speed camera image

After the crack propagation slowed down, the specimen was put aside while the wedge was still inserted. Then, the position of the crack front was marked on the specimen manually. After the crack propagation stopped, a picture of the specimen was taken and marked crack lengths at different time values were calculated by the image processing software (PFV, high speed camera software). All the tests were performed at 22°C.

Results and Discussion

Gel Content

The gel contents of the organogels were calculated by Equation 3-19.

$$\%\ gel\ fraction = \frac{M}{M_0}\ x\,100 \qquad (3\text{-}19)$$

where M_0 is the calculated initial monomer weight (without solvents) and M is the weight of dry crosslinked polymer after extraction.

During the solvent extraction experiments, the unreacted residual monomers and the solvents in the organogel dissolved in the extraction solvent. Therefore, the amount of the crosslinked polymer in the organogel was calculated. A minimum gel fraction percentage of 80.8% was obtained for the lowest curing time (150s), a maximum gel fraction percentage of 97.7% was obtained for the highest curing time (1800s). Figure 3-16 shows the effect of curing time on the gel contents of the organogels.

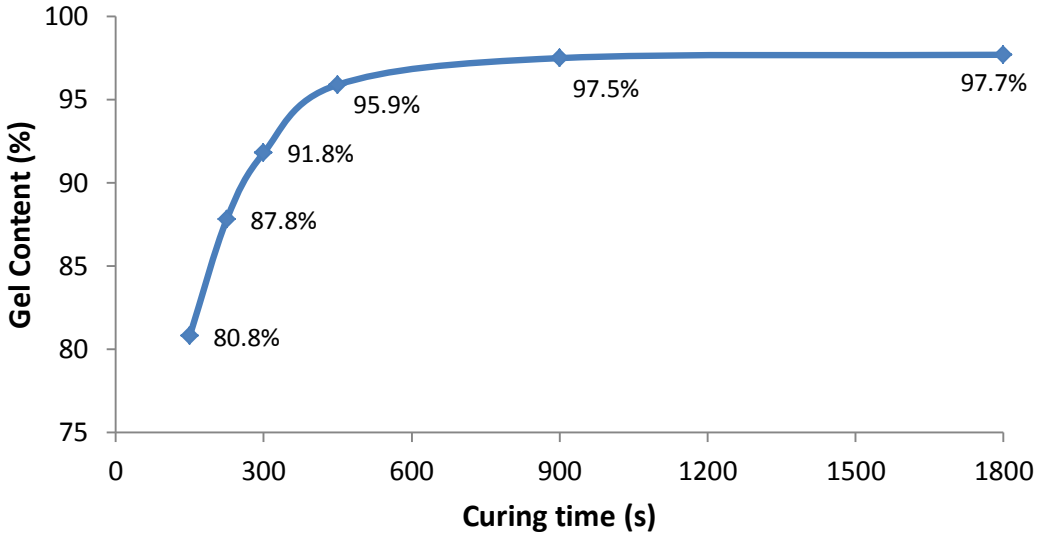

Figure 3-16: Effect of curing time on gel contents of the silicone semi-IPN organogels

Gel content of the organogel increased significantly with the increasing photo-curing time. However, after 450s, the increase in the gel content was very low; therefore, polymerization was mostly complete after 450s. Dolez et. al studied the effect of photo-curing time on triethylene glycol dimethacrylate and bisphenol-A diglycidyl ether dimethacrylate based acrylic resins and showed a very similar time dependence of the curing behavior [21].

Uniaxial Tensile Behavior and Shear Modulus

Stress-strain plots of the organogels as a function of curing time were obtained. Since these materials show a non-linear stress-strain behavior, neo-Hookean model was used to characterize the tensile properties of the organogels (Equation 3-11). For the each curing time, at least 5 different trials were performed and repeatable stress-strain plots were obtained. Representative stress vs. neo-Hookean deformation metric ($\lambda - \frac{1}{\lambda^2}$) plots for the different curing times are shown in Figure 3-17.

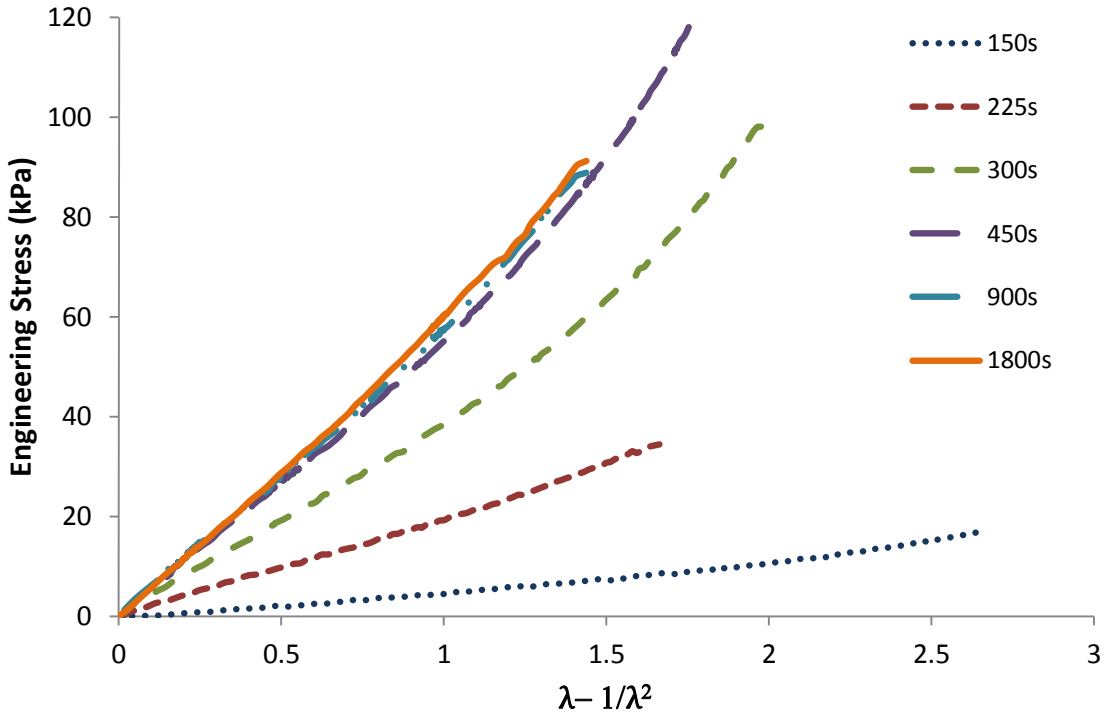

Figure 3-17: Stress vs. neo-Hookean deformation metric plots of different curing times

As the curing time increased, stresses required to stretch the samples increased significantly. However, after 450s curing time, the stress-strain behavior was almost the same. Shear modulus values of the organogels were calculated using Equation 3-11. The stress vs. $\lambda - \frac{1}{\lambda^2}$ plots were linear within the range of 40% strain, therefore, slopes of the plots were obtained from this region to calculate the shear modulus. Figure 3-18 shows the effect of curing time on shear modulus of the materials.

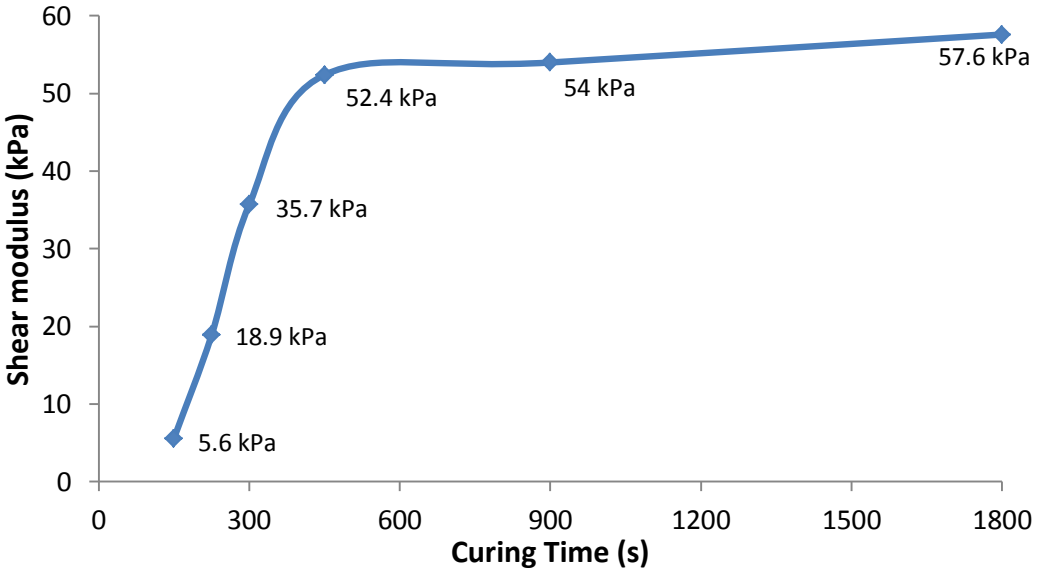

Figure 3-18: Effect of curing time on shear modulus of the organogels

A 5.6 kPa shear modulus was obtained for the minimum curing time which is a relatively low value for the polymeric materials in the rubbery plateau. However, as the curing time increased, shear modulus values increased significantly until 450s curing time. For the highest curing time (1800s), shear modulus value was 57.6 kPa. It should be noted that the effect of curing time on the gel contents showed the same trend with the effect on the shear modulus values. The shape of the plots showed in Figure 3-16 and Figure 3-18 are substantially similar. Curing time may increase both the extent of reaction and the crosslink density of the materials. The gel content study mostly investigated the effect of curing time on the extent of reaction. However, both the extent of reaction and the crosslink density have significant effects on the shear moduli of the materials. Therefore, curing time showed higher impact on the shear moduli.

Thermo-mechanical Behavior and Viscoelastic Properties

The effect of curing time on the thermomechanical behavior and the viscoelastic properties of the organogels were obtained by a dynamic mechanical analyzer in shear deformation mode. Shear

storage moduli and tan delta values were plotted as a function of temperature. Figure 3-19 shows the shear storage modulus plots of the organogels cured for different times.

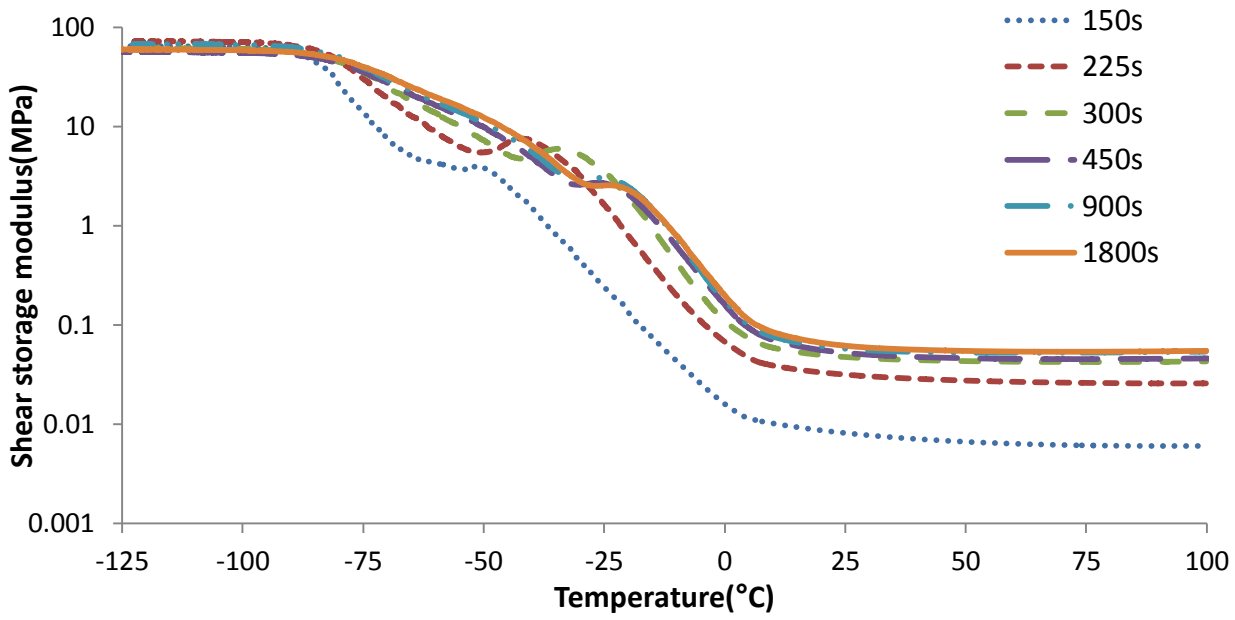

Figure 3-19: Shear storage plots of different curing times at 1Hz deformation frequency

Figure 3-19 shows that rubbery shear storage moduli of the organogels increased with the increasing curing time. However, the glassy modulus was not significantly affected by the changes in the curing time. At the glassy state, polymer chains do not have segmental motions therefore motions of the chains are very restricted. Since the molecules act as frozen in this state, changes in the crosslink density did not affect modulus. However, at the rubbery state, polymer chains are mobile and the stiffening effect of the crosslink density would be prominent with the higher curing times. Gent et al. studied the effect of crosslink density on rubber and found that the rubbery moduli are affected by a factor of 6 whereas the glassy moduli of materials with different crosslink densities were very close to each other [46]. Similar behavior was also shown by Tobolsky. Crosslinker ratio ranged from 1.07% to 100% and storage moduli obtained as a

function of temperature. Even though the rubbery moduli of the materials varied significantly, the glassy moduli of the materials were close to each other[52].

On all of the storage modulus plots, there was an extraordinary increase in the storage modulus on the leathery region. For example, the increase was at around -50°C and -25°C for the 150s curing time and 300s curing time respectively. The increase is about the phase changes of the solvent in the material and will be discussed in detail in Chapter 4.

Dynamic mechanical analysis is a widely used technique to characterize the thermal transitions of the materials. Figure 3-1 shows representative storage modulus and tan delta plots indicating some of the thermal transitions. Tan delta plots of the organogel materials (Figure 3-20) were obtained and α transitions of the materials were mainly investigated.

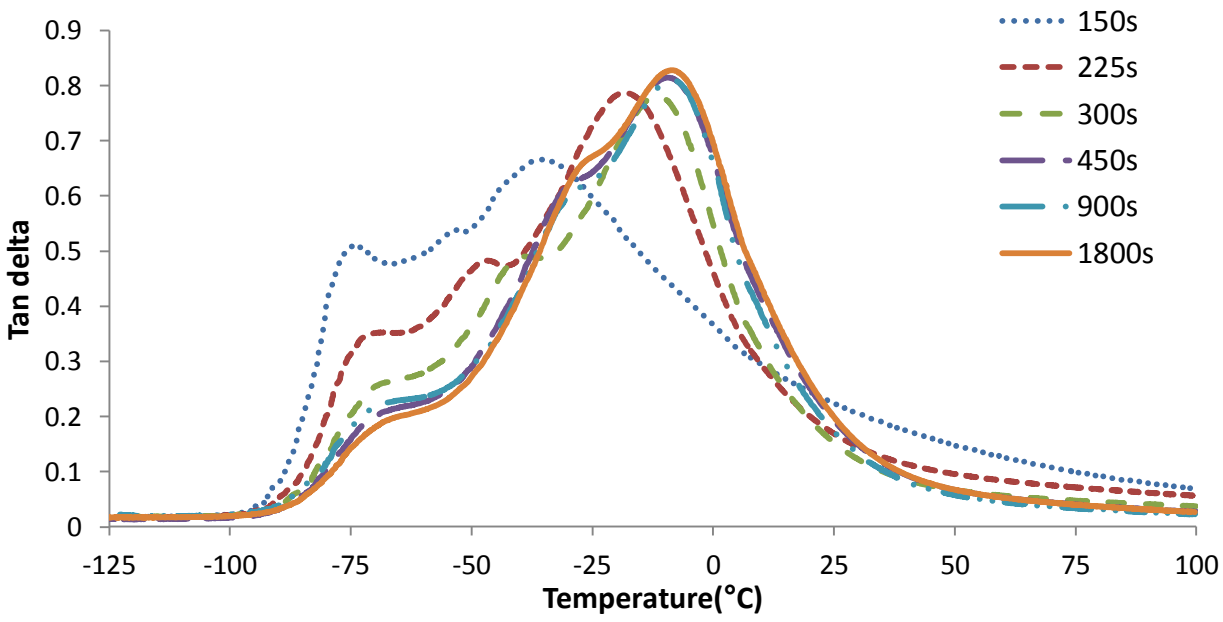

Figure 3-20: Tan delta plots of different curing times obtained at 1 Hz frequency

Figure 3-20 shows that the organogel materials exhibited three different thermal transitions (α, β,γ transitions) for all the curing times. It should be noted that the transition temperatures shift to

higher temperatures as the curing time increases. Increase in the thermal transition temperatures with the increasing curing time is related with the decrease in the molecular mobility. As the curing time increases, the extent of reaction and the crosslink density increases so the mobility of the polymer chains decrease. Therefore, more energy is needed to initiate the short range and the long range segmental motions of the polymer chains and the thermal transitions occur at higher temperatures. The effect of curing time on α transition temperatures of the organogels is shown in Figure 3-21.

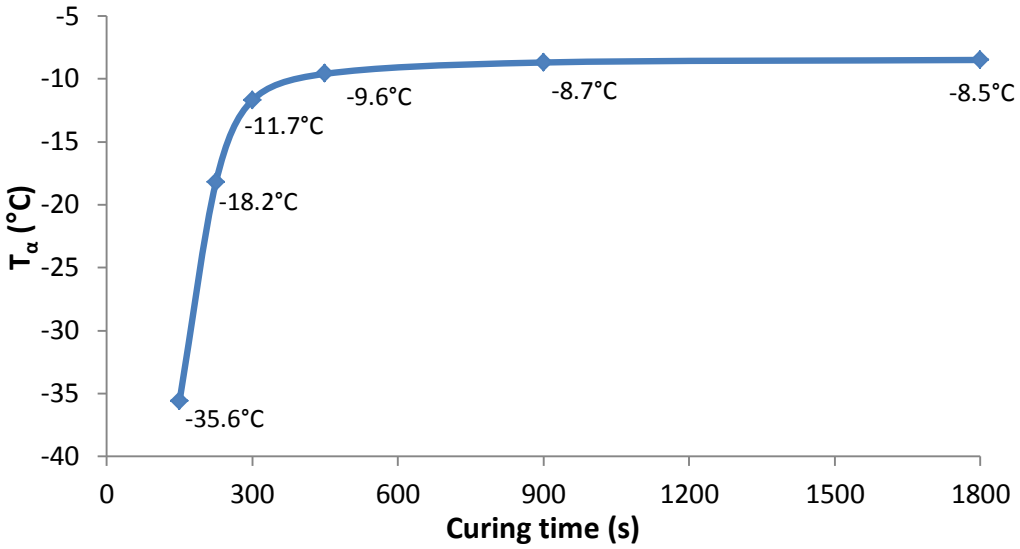

Figure 3-21: Effect of curing time on transition of the organogels

The change in the glass transition (generally α transition) temperature with the increasing crosslink density previously discussed for many different crosslinked polymer systems[53]. Figure 3-21 shows that the α transition of the organogels significantly shifts to higher temperatures with the increasing curing time until 450s curing time. As mentioned above, the changes in the extent of reaction and the changes in the crosslink density of the organogel may affect the mobility of the polymer chains in the organogel, resulting differences in the thermal transition temperatures. An α transition temperature of -35.6°C was observed for the lowest

curing time and the temperature increased significantly until 450s curing time since the curing is almost complete at this curing time.

At low temperatures and at temperatures above 25°C, higher tan delta values were observed at lower curing times, especially for the 150s curing time. Due to the lower crosslink density, higher viscoelastic dissipation was observed. Increasing viscoelastic dissipation with the decreasing crosslink density was previously discussed on rubber elastomers[46]. The effect of the viscoelastic dissipation on the fracture properties will be discussed on the following sections.

Cohesive Fracture Properties

The effective moduli of the organogels were obtained to implement the relaxation effects into the fracture energy calculations. Figure 3-22 shows the effective modulus plots of the organogels as a function of time. The fits of the each plot were obtained and the time dependent modulus values were calculated accordingly to calculate the SERR. It is also important to note that the effect of the curing time on the effective modulus of the materials were consistent with the other constitutive properties.

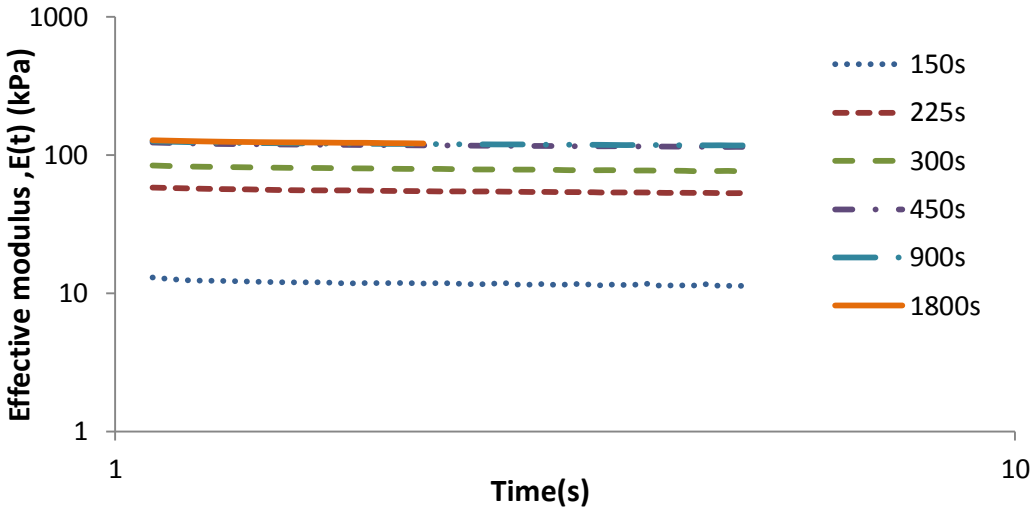

Figure 3-22: Effective modulus plots

To characterize the cohesive fracture properties, the pre-cracked samples were stretched to 40% of their initial height in 1 second and strain level kept constant until the crack propagates across the entire length of the sample. For all of the curing times, steady-state crack propagation was observed. Figure 3-23 shows the diagram of the constrained fracture test specimen. Regions 1 and 3 were ignored for the calculations of crack propagation rate and the strain energy release rate (SERR) since these regions may exhibit complex strain states because of the edge effects. Only data from region 2 was analyzed.

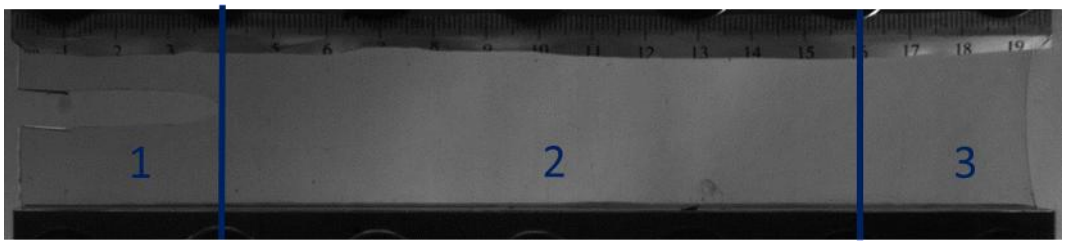

Figure 3-23: Constrained fracture test specimen fracture regions

SERR of the materials were calculated using Equation 3-12. To characterize the effect of curing time on the cohesive fracture behavior of the materials, SERR vs. crack propagation rate plots

were obtained (Figure 3-24). Due to the differences in the extent of reaction, crosslink density and viscoelastic dissipation, fracture behavior affected significantly by the curing time.

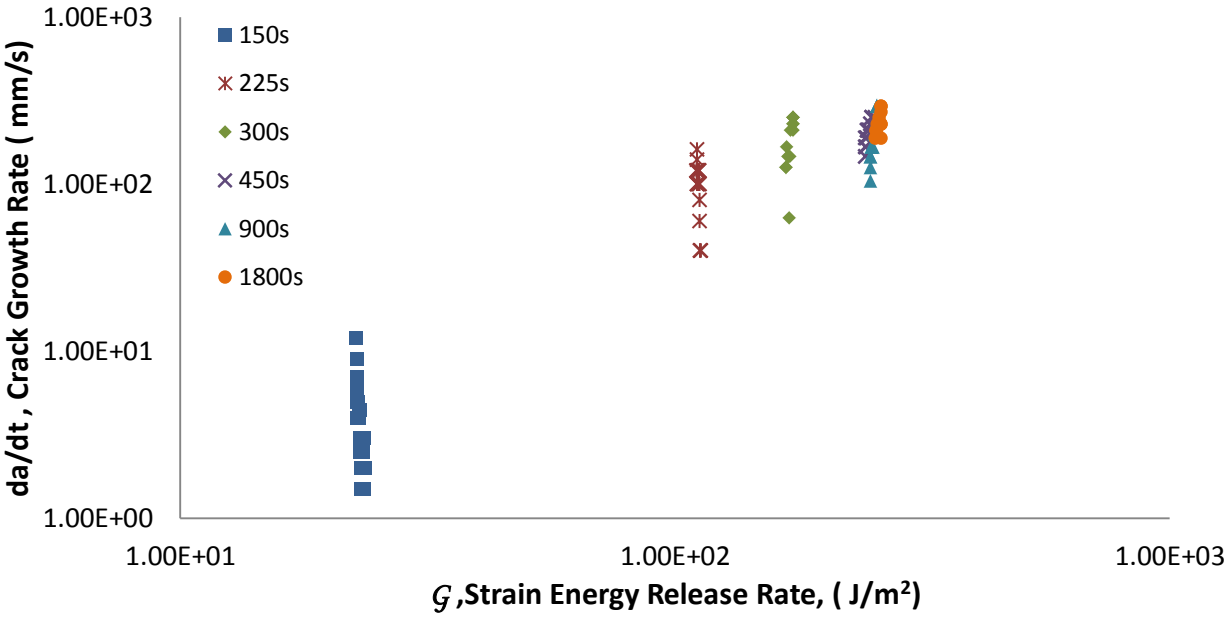

Figure 3-24: Effect of curing time on the cohesive fracture properties

SERR of the organogels increased with the increasing curing time due to the increase in the stiffness of the materials. However, crack propagation rate also increased significantly since curing time affects the crosslink density of the material making them more brittle. At higher curing times, organogels store more deformation energy elastically, which may act as a driving force for the propagation of the crack. At lower curing times, materials dissipate more energy therefore crack growths rates were substantially lower, especially for the 150s cured organogel. When the same strain profile was applied to the pre-notched specimens, complete fracture of the 150s cured sample took 50 seconds whereas it was only 1.8 seconds for the 1800s cured specimen. In conclusion, both SERR and crack propagation rate increased with the increasing curing time. After 450s curing, increase in the curing time did now show any significant effect on the fracture properties of the organogels since the material was almost fully cured at 450s.

Adhesive Fracture Properties

Wedge tests were used to characterize the effect of curing time on the adhesive fracture properties of the organogels. Strain energy release rates (SERR) of the interfacial fracture between the organogel and the cyclo-olefin polymer were calculated using Equation 3-14 and plotted as a function of crack growth rate (Figure 3-25).

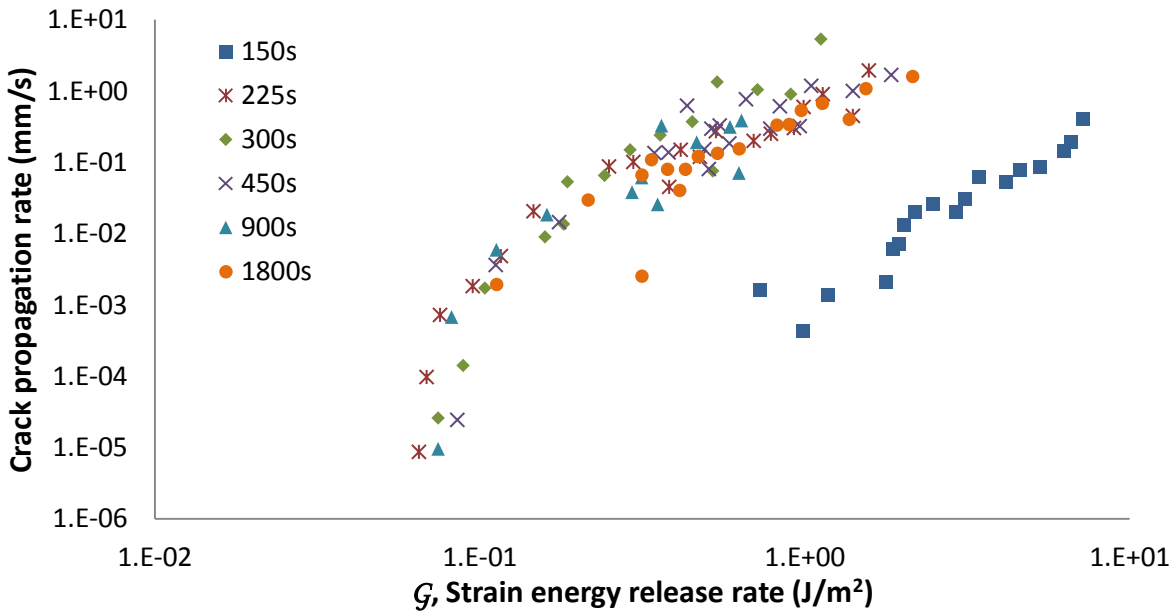

Figure 3-25: Effect of curing time on the adhesive fracture properties

For the 150s sample, interfacial crack did not propagate as much as the other curing times; therefore, data could not be collected at lower crack propagation rates. Adhesive fracture properties of all the curing times were found to be almost the same except the 150s curing time. Previously, it was shown that the 150s curing time dissipates more energy upon deformation and shows less brittle cohesive fracture behavior than the other curing times. According to the Lake-Thomas theory[44], materials with lower crosslink densities should have higher fracture energy. Even though the 150s sample has the lowest stiffness among all the materials, the adhesive SERR values of this material were the highest at a given crack propagation rate due to the less

crosslink density and high viscoelastic energy dissipation. It is important to note that viscous stretching may confound the results, shifting the calculated SERR values to higher values.

Conclusions

This chapter discusses the effect of curing time on the gel content, uniaxial tensile, dynamic mechanical, cohesive and adhesive fracture properties of silicone semi-IPN organogels. It is shown that there are several factors that might be affected by the changing curing time which significantly play a key role on some of the properties of the materials. Firstly, gel contents of the organogels were obtained by solvent extraction method. Results showed that the extent of reaction significantly increases as the curing time increased until 450s. Constitutive mechanical properties showed very consistent results with the gel content results. Due to the higher extent of reaction and increase in the crosslink density, shear modulus values calculated by uniaxial tension tests were gradually increased with curing time until 450s. After this curing time, the changes were very small since the curing was almost complete at 450s. Similar effects were also observed on the dynamic mechanical properties. As the crosslink density and the extent of reaction increased, the mobility of the polymer chains decreased. Therefore, thermal transition temperatures of the materials shifted to higher temperatures as a result of the increase in the curing time. It is important to note the effects of curing time on the constitutive properties are considerably analogous and the shape of the gel content, shear modulus and α transition temperature plots were substantially similar (Figures 3-16, 3-18 and 3-21, respectively).

The cohesive fracture properties showed important sensitivity to curing time until 450s. Higher SERR values were obtained for the higher curing time specimens due to the increasing stiffness of the organogels. However, as the curing time increased, crack growth rate of the materials increased significantly. Elastically stored energy at higher crosslink densities or high viscoelastic

dissipation at lower curing times are the possible reasons for different cohesive fracture behavior of these materials at different curing times.

The adhesive fracture properties were obtained by wedge tests. The organogel cured for 150s showed a decade higher strain energy release rate values since it dissipates more energy than the other curing times. The adhesive fracture energy values are lower than the cohesive energy values. Therefore, if these specimens are debonded from a cyclo-olefin polymer surface, the fracture will most likely to occur adhesively. However, since 150s curing time showed the lowest cohesive and highest adhesive fracture energy values, a possible adhesive to cohesive fracture transition may occur during debonding of these materials.

Chapter 4 : Thermal Properties and the Effect of Solvent Crystallization

Introduction

In three dimensional polymer organogels, relatively small organic solvent molecules are immobilized within the porous structure of the gel network. Therefore, these types of materials are regarded as "semi-solid". However, they have rheological behavior of solids since physical interactions between the polymer network and the solvents prevent the flow of the liquid phase[54, 55].

In the literature, organogels are divided into mainly two categories; physical organogels and chemical organogels. Physical organogels are formed by thermo-reversible aggregation of solvent molecules whereas chemical organogels are formed by entrapment of solvent molecules in the three dimensional crosslinked network structures [56-58]. Since the chemical gels entraps solvent molecules within the covalently crosslinked networks, they are more robust and resistant to physical deformations[59]. According to these definitions, the silicone semi-IPN material used in this study is a chemical organogel which crosslinked *in situ* in the organogel solvent.

Markovic et al. studied the thermal properties of different chemical and physical organogels and showed the kinetics and the thermal behavior of solvents within the polymer network structure [56-58]. In one study, they studied the chemical organogels formed by *in-situ* crosslinking of siloxane monomers in the presence of benzene solvent. As the network scaffolding increased, crystallization and melting temperatures of the benzene shifted to lower temperatures and respective exothermic and endothermic peaks became broader [58]. Roberts et al. studied the thermal properties of core-shell rubber/styrene gels. In this study, rubber/PMMA system was used as the absorbing polymer network and styrene monomer was the gel solvent. Similar to the

previous study[58], they showed that the melting and freezing points of the styrene shift to the lower temperatures. On differential scanning calorimetry (DSC) plots, neat styrene monomer showed a sharp melting peak whereas the melting peak of styrene was broader when it was present in the rubber network. They also showed an unusual crystallization behavior of the styrene when it was in the gel network. The monomer crystallized during the heating scan but not during the cooling scan of the DSC. During cooling, crystallization was kinetically hindered since the time window between the onset of crystallization and the gel system vitrification was small. As the organogel was heated through the glass transition temperature of the material, the mobility of the solvent molecules increased, therefore solvent could crystallize upon heating. Crystallization upon heating from glassy state to amorphous state is called "cold crystallization"[60]. Both the structure of gels and the interaction between solvents and polymer network might result cold crystallization of a solvent.

The interaction of diluents or solvents with the polymer network in an organogel might cause melting and crystallization point depression of the diluent or solvent. Vikki et al. studied the thermal properties of resorcinol in polyaniline sulfonic acid solvated polymer system. Due to the strong hydrogen bonding and phenyl-phenyl interactions between the resorcinol and the polymer complex, the melting temperature of the resorcinol shifted to lower temperatures. For example, pure resorcinol has melting point of 115°C, however, melting point of the resorcinol decreased to 98°C when it was present in 40/60 w% polyaniline/resorcinol mixture. Resorcinol also showed a cold crystallization behavior[61].

Differential scanning calorimetry (DSC) is one of the most widely used techniques to characterize the thermal properties of materials. Since DSC measures the changes in the heat flow as a function of temperature and time, a thermal transition should result endothermic or

exothermic changes in the heat flow in order to be characterized by a DSC. This technique can provide qualitative and quantitative information about glass transition, melting, crystallization, curing, reaction kinetics and specific heat capacity of materials. “Heat flux DSC” and “power compensation DSC” are the two basic types of differential scanning calorimeters. The heat flux DSC measures the enthalpic difference by measuring the temperature difference between a sample and a reference whereas the power compensation DSC keeps the temperature of a sample and a reference at the same temperature and measures the electrical resistance to calculate the enthalpy difference[62]. In this thesis, a heat flux DSC (TA Instruments) is used.

Conventional DSC measures the total heat flow associated with thermal transitions during DSC experiments. In addition to the conventional method, modulated DSC (MDSC) separates the total heat flow signal to its thermodynamic and kinetic components. Therefore, overlapping complex transitions such as crystallization and melting can be captured. Basically, MDSC applies a changing heating rate on top of a linear heating rate in order to measure heat flows that respond to the changing heating rate. Equation 4-1 shows the mathematical representation of the heat flow[63].

$$\frac{dH}{dT} = C_p \frac{dT}{dt} + f(t,T) \tag{4-1}$$

where $\frac{dH}{dT}$ is the heat flow out of the sample, $\frac{dT}{dt}$ is the heating rate, C_p is the thermodynamic heat capacity, t is the time, T is the absolute temperature and $f(t,T)$ is the function of time and temperature which controls the kinetic response of any transition [63]. Therefore, the heat flow has two components; heating rate dependent and absolute temperature dependent. Depending on the effect of the heat flow component, transitions are called as reversing and non-reversing,

respectively. For example, glass transition is a reversing transition whereas cold crystallization is a non-reversing transition [63, 64].

Crystallization behavior of materials can be significantly affected by the heating rate/cooling rate of a DSC experiment. Generally, as the heating rate increases, cold crystallization temperatures shift to higher temperatures [65, 66]. Since cold crystallization occurs when the samples are heated from glassy state to amorphous state, cold crystallization temperatures should be dependent on the segmental mobility of the network[67]. Marosi et al. showed that both glass transition temperatures and cold crystallization temperatures shift to higher temperatures with the increasing heating rate[67].

Baba et al. studied the relationship between the solvent freezing point depression and the network structure of solvated gels. Volume fraction of the ethylene propylene diene monomer (EPDM) elastomer was varied by changing the photo-oxidation time and the relationship between the volume fraction and the freezing enthalpy investigated. As the photo-oxidation time increased, the volume fraction of the gel increased. The network of the gel became more confined and crystallization of the solvent (heptane) inside the gel decreased due to the increasing confinement. [68]. Therefore, thermal behavior of a solvent can be used to obtain information about the polymer network structure such as degree of crosslinking and mesh sizes and distributions. For example, Honiball et al. proposed a method in which solvent freezing point depression of swollen rubbers was used to calculate the crosslink densities of materials[69].

The state of water in hydrogels can be separated into three categories: (1) free, (2) freezing bound, and (3) non-freezing bound water. The free water does not form hydrogen bonding with the hydrogel therefore its characteristic properties such as crystallization temperature,

crystallization enthalpy or shape of the DSC curves are similar to those of pure water. Freezing bound water weakly interacts with the polymer network. Non-freezing bound water strongly interacts with the polymer through hydrogen bonding and does not freeze when the hydrogel is cooled down to temperatures below 0°C [70-73]. Depending on the interaction type and the strength of a solvent and an organogel polymer, thermal properties of the solvent can be significantly different. Previously, the free and bound states of solvents in organogels were investigated by DSC studies [56-58].

When a polymer is solvated with a liquid such as an organic solvent or water, glass transition temperature of the network decreases and the material becomes softer and flexible since these low molecular weight liquids disrupt the intermolecular interactions between the polymer chains. Therefore, these liquids are used to plasticize rigid polymers to make them useful for practical purposes[74]. Previously, it was shown that swollen rubber networks have very low glass transition temperatures compared to dry rubber when the swelling solvent is in the liquid state. However, if a solvent in a gel freezes, it shows higher glass transition temperatures, close to the glass transition temperature of dry polymer. Therefore, plasticizer effect of the solvent diminishes when the phase of the solvent changes to the solid state from the liquid state [75]. Even though the thermal properties of solvents in swollen gel networks are extensively studied, the research on the effects of thermal changes such as phase change of solvents on different material properties is limited. If a solvent in a gel freezes, the mechanical properties of the system should change significantly since the solvent in the liquid phase will not act as a plasticizer anymore. This chapter extensively discusses the thermal behavior of the solvent-A in the silicone semi-IPN organogel material and its subsequent effects on the constitutive properties of the material.

Experimental Methods

Differential Scanning Calorimetry (DSC)

Conventional DSC

In this chapter, DSC was used as the main tool to characterize the thermal properties of the silicone semi-IPN organogel. A heat flux DSC (TA Instruments Q-2000) was used to measure the changes in the heat flow as a function of temperature and time. About 10 mg of organogel sample was cut by a razor blade from a bulk sample prepared in sandwich molds (Chapter-2) and weighed out using scales capable of being read to four decimals. Then, the specimen was placed on to an aluminum DSC pan (TA Instruments) and capped with a smaller aluminum lid and crimped. The empty DSC pan and lid were approximately 30mg. An empty DSC pan and a lid were used as a reference during the DSC measurements.

DSC experimental conditions such as heating rate, minimum and maximum heating/cooling temperatures were different for various experiments and these details will be provided in the results section with the corresponding DSC plot. Two heating and cooling cycles were performed and the second heating and cooling cycles were analyzed since the first cycles may show some aging effects.

Modulated DSC (MDSC)

MDSC experiments were performed to investigate the overlapping transitions during the DSC experiments. The same TA Q-2000 DSC was used to perform the modulated DSC experiments. The heating rate was 5°C/min and the temperature range was -80°C to 50°C. Specimen preparation for the modulated DSC was the same with the conventional DSC. Temperature modulation was ±1.00°C every 60 seconds.

Dynamic Mechanical Analysis

The details about the DMA with shear sandwich clamps were given in Chapter-3. In this chapter, DMA was used to characterize the effects of thermal changes such as crystallization of the solvent on the thermo-mechanical properties of the materials. Depending on the experiment type, different heating rate, minimum cooling and maximum heating temperatures were used. These experimental conditions will be given with the corresponding DMA plots.

Optical Microscope with a Thermal Stage

To investigate the thermal changes such as crystallization and melting, a thermal stage (Linkam THMS600) attached optical microscope (Nikon Eclipse LV 100) was used in transmission mode. Thin films of organogel was cured between plastic molds and placed on to microscope cover glasses. A cooling pump filled with liquid nitrogen was used to cool the specimens (Figure 4-1).

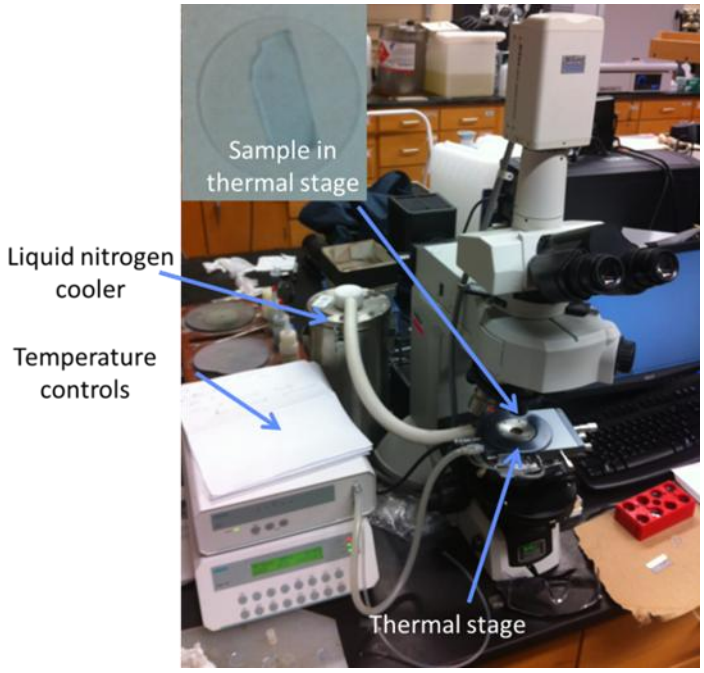

Figure 4-1: Optical microscope with the Linkam thermal stage

During the experiments, temperature of the specimens was equilibrated at -70°C and the samples were heated to room temperature at 5°C/min heating rate. The optical microscope was set to acquire images at every 15 seconds. An example microscope image with a scale bar is shown in Figure 4-2. The images in the results section do not have the scale bars but the magnification and the scale of those images are the same with the one in Figure 4-2.

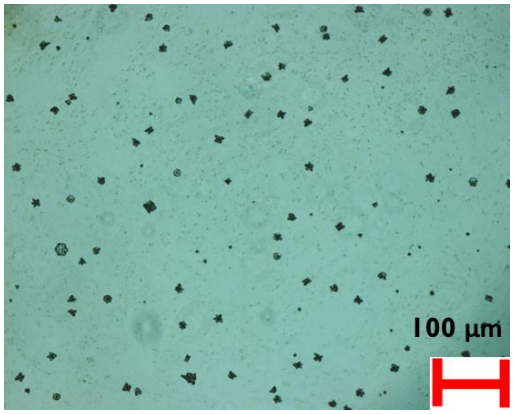

Figure 4-2: Example optical microscope image with a scale bar

Results and Discussion

Crystallization and Melting Behavior of Solvent-A

DSC experiments showed that one of the components of the semi-IPN organogel crystallizes and melts during the heating scan. The cold crystallization temperature (T_c) was -24°C and the melting temperature of the crystallized component was -8°C for 900s cured specimen (Figure 4-3).

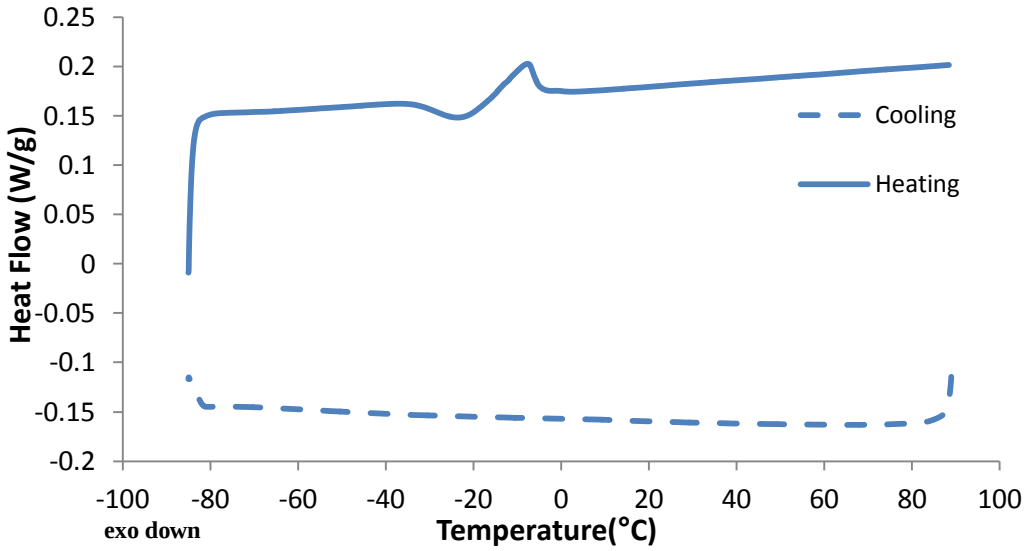

Figure 4-3: DSC plot of 900s cured sample

Crystallization of the solvent was hindered during cooling since the mobility of the network reduced and did not let the solvent to crystallize. However, during heating, the material was able to crystallize once the network became mobile again which kinetically allowed the crystallization of the solvent.

To investigate the crystallization process, heating experiments were performed under optical microscope. When the sample was equilibrated at -70°C, some crystals grew. However, these crystals melted at around -30°C and new, smaller particles started to form. These particles melted at around -10°C. Figure 4-4 represents the microscopy images of the specimen at different temperatures, showing the two melting processes observed within the organogel material.

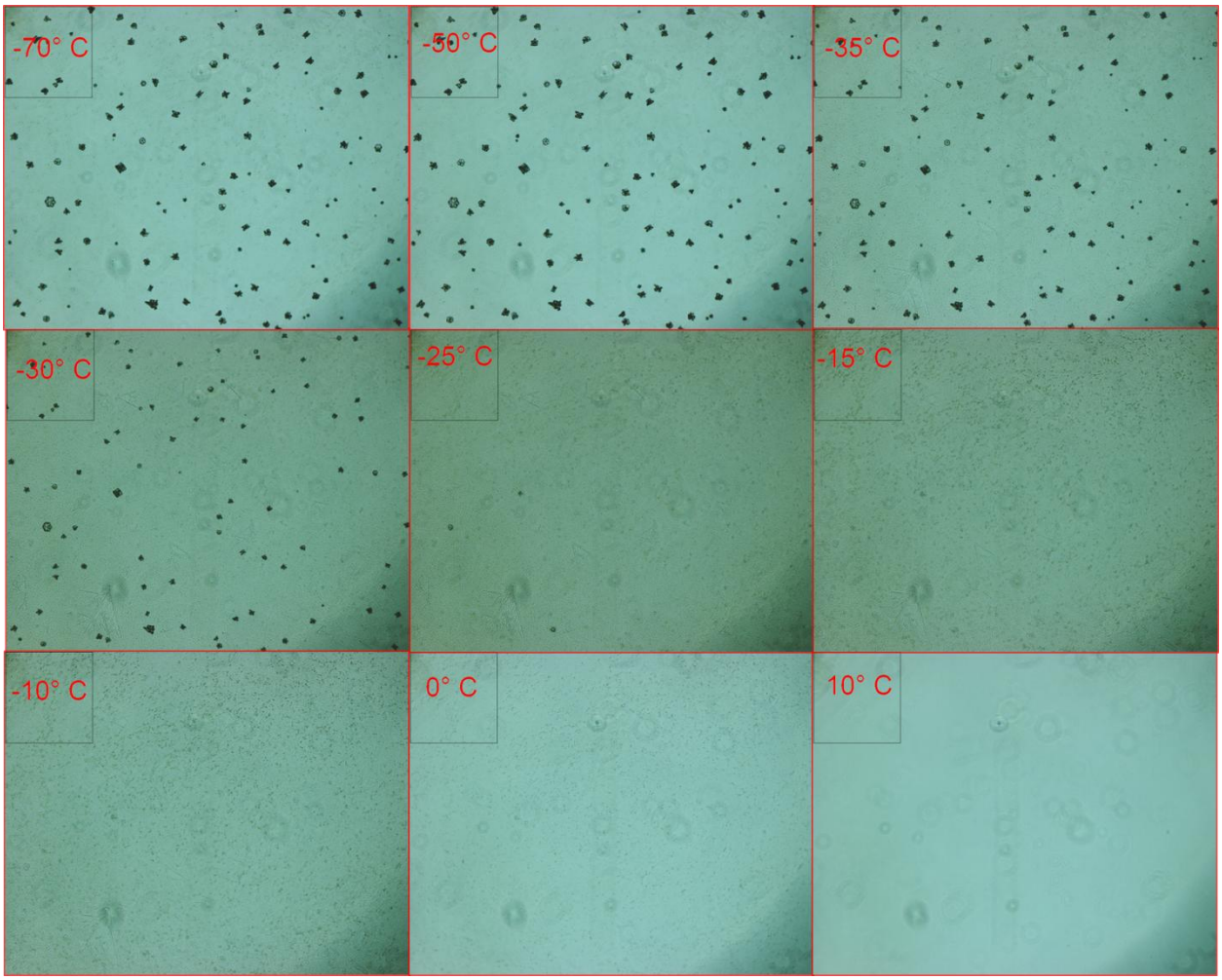

Figure 4-4: Heating microscope images of 900s cured organogel

Initially formed crystals at -70°C and their melting at around -30°C did not show up on the conventional DSC plot (Figure 4-3). When these crystals melted at around -30°C, a new crystallization process started. The newly forming particles were smaller in size. However, they were all around the specimen making the specimens darker at corresponding temperatures (Figure 4-4). As soon as these particles melted, the sample became light-colored again. The melting at -30°C did not show up on the DSC plot because the melting overlapped with the crystallization which started at around the same temperatures. To investigate the overlapping melting behavior, MDSC experiment was performed (Figure 4-5).

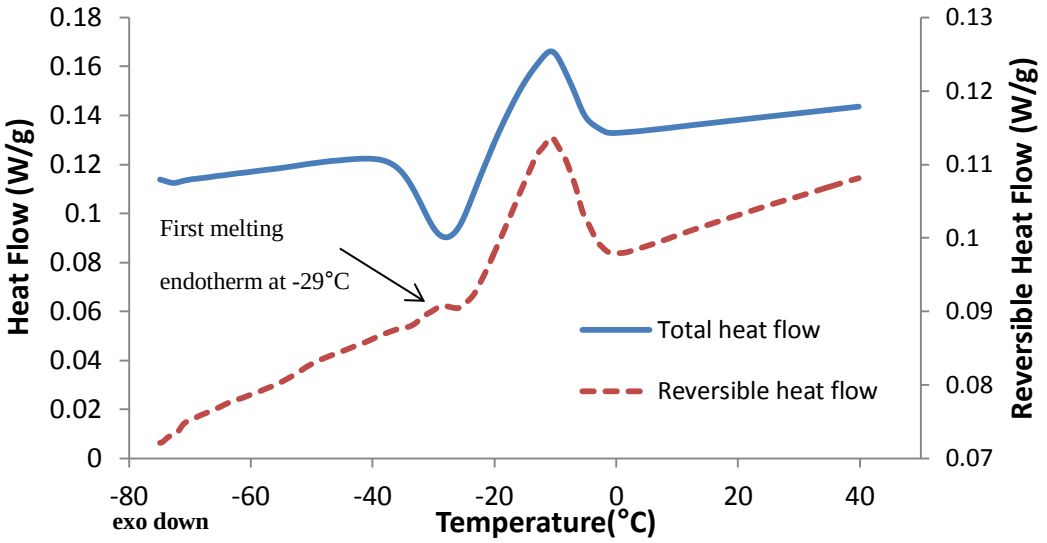

Figure 4-5: MDSC second heating scan of 900s cured sample

Figure 4-5 shows that there is a small endothermic peak at -29°C on the reversible heat flow plot. This endotherm is associated with the first melting of the crystals which initially formed while the sample was equilibrated at -70°C. The same experiments were also performed with the 225s cured sample to compare the thermal behavior by the thermal optical microscope and the MDSC. Figures 4-6 and 4-7 show the microscopy images and the MDSC plots of 225s cured sample respectively.

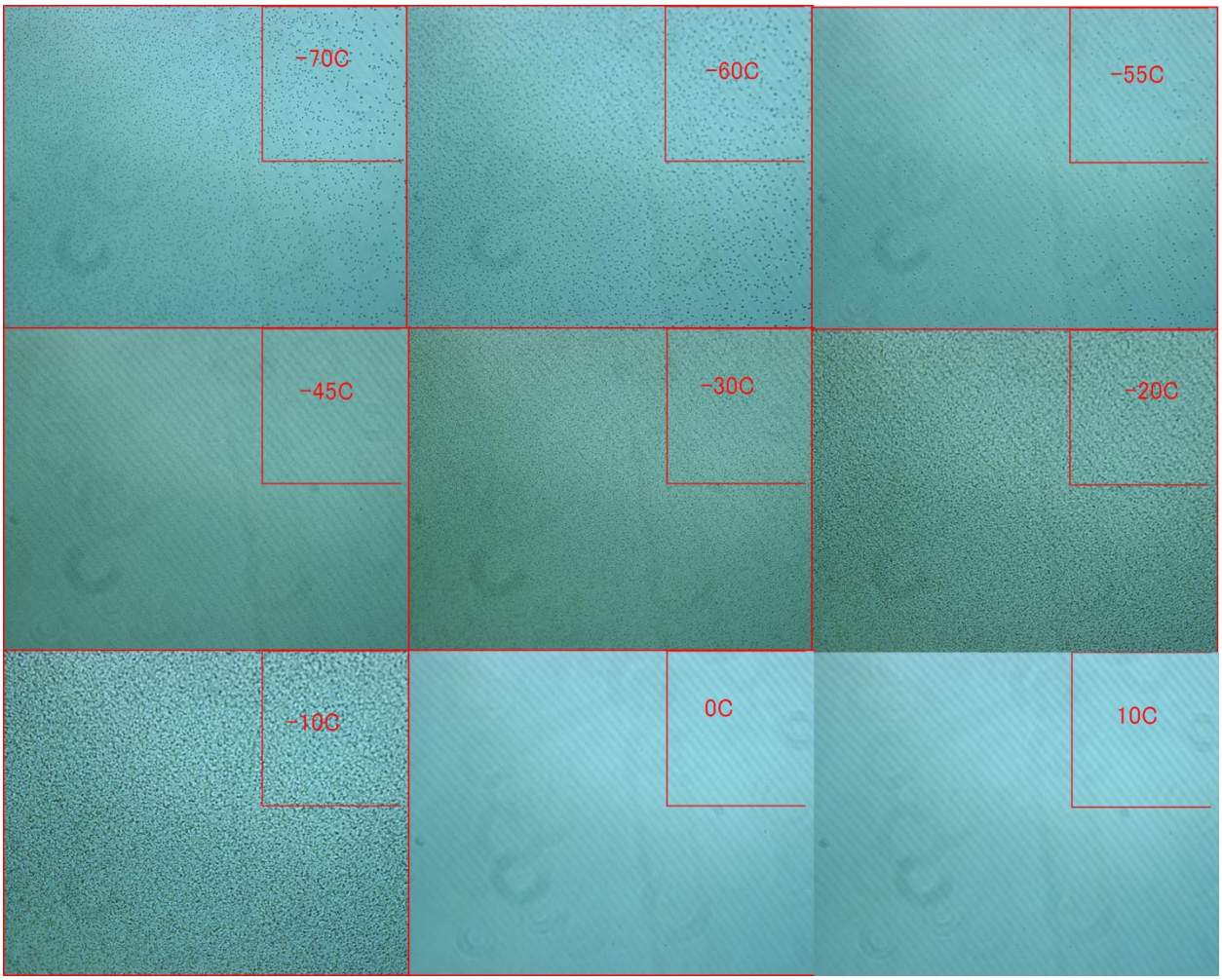

Figure 4-6: Heating microscope images of 225s cured organogel

According to Figure 4-6, the crystals first melted at around -55°C and after this temperature, the images became darker, indicating new freezing component in the organogel. These particles started to melt at around -10°C.

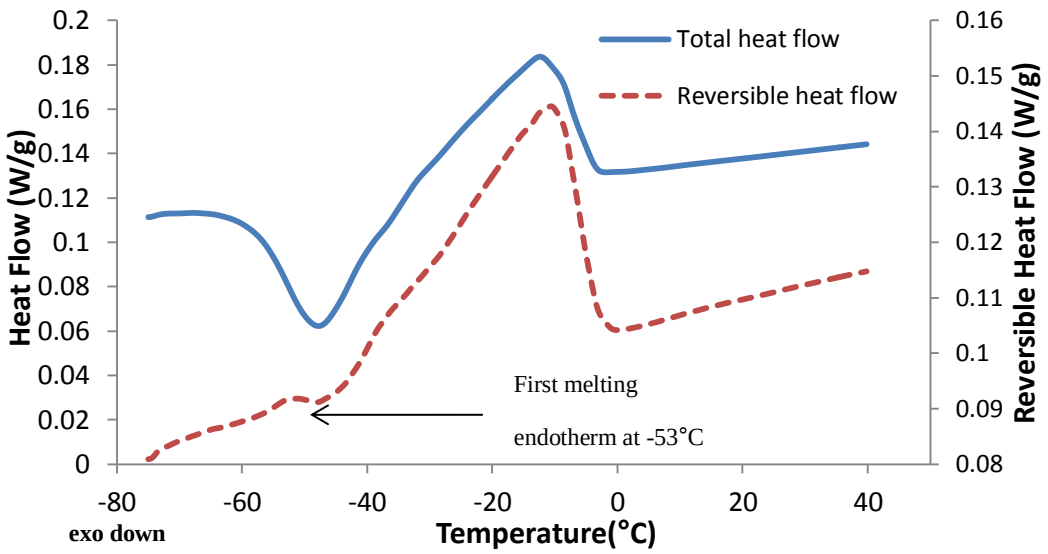

Figure 4-7: MDSC second heating scan of 225s cured sample

Small endotherms which overlapped with the crystallization peaks were captured on the reversible heat flows at -29°C and at -53°C for the 900s and 225s cured samples respectively (Figure 4-5 and Figure 4-7). These melting temperatures exactly matched with the first melting temperatures observed by the optical microscope (Figure 4-4 and Figure 4-6).

Water or solvents may show more than one melting processes when they are present in hydrogels [70-73] or in organogels [56-58] respectively. This behavior is due to the type and the strength of intermolecular interactions between low molecular weight solvents/diluents and the polymer network. Also, heterogeneity in the network such as different mash sizes may cause different melting processes[68]. Two different melting processes observed with the solvent in the organogel network may be caused by different types and strengths of the interactions and/or different mash size of the crosslinked semi-IPN network.

To investigate the melting component in the organogel network, a monomer mixture without Solvent-A was prepared. The total solvent content in the mixture was kept the same by adding

extra Solvent-B. The melting point of Solvent-B is below the test range temperatures of these experiments, so it should not show any melting peaks at around -10°C. An optical microscopy and a DSC study were performed using the formulation without Solvent-A to investigate the type of the freezing component.

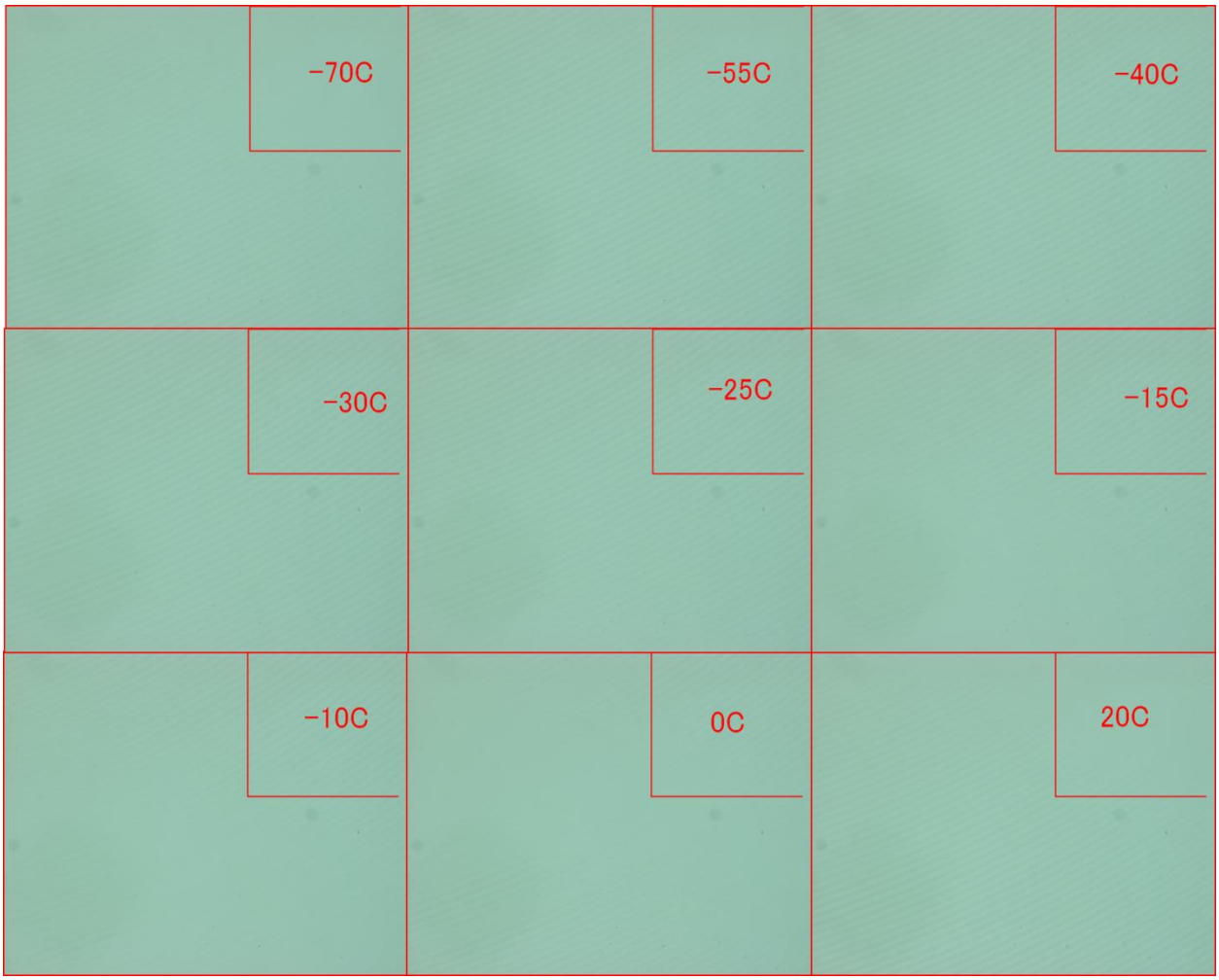

Figure 4-8: Heating microscope images of 900s cured formulation without Solvent-A

Unlike Figure 4-4 and 4-6, there were no traces of crystallization or melting in Figure 4-8 since Solvent-A is the crystallizing component in the organogel. These results were also supported by the DSC experiments (Figure 4-9).

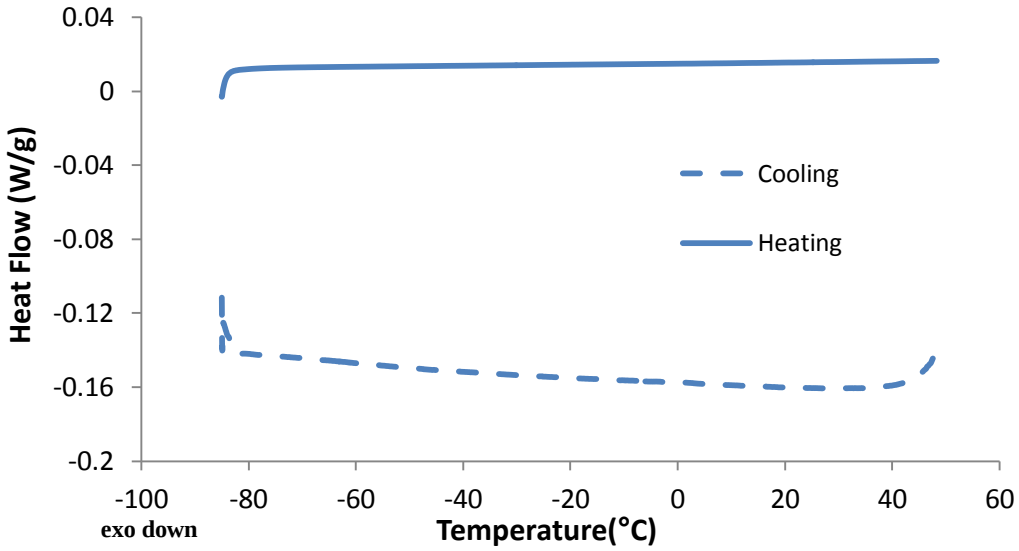

Figure 4-9: DSC plot of 900s cured organogel without Solvent-A

The organogel specimen without Solvent-A did not show any crystallization/melting during the thermal microscopy and DSC experiments. Therefore, it is concluded that Solvent-A was the component that showed crystallization and melting during the experiments.

Microscopy images showed two different melting processes and the results were supported by MDSC experiments. When the areas under the melting peaks of the first and the second melting were compared, the area under the second melting curve (at -8°C) was much larger than the area under the first melting curve (at –29°C) indicating that the amount of the second crystallized component was much larger than the amount of the first crystallized component. Therefore, only the second melting component (the only melting peak observed by the conventional DSC experiments) will be discussed on the following experimental results.

Melting Point Depression of Solvent-A

Solvents can show melting points at lower temperatures than their pure melting points when they solvate a polymer system. Melting point depression is mainly due to intermolecular interactions

between solvent molecules and a polymer network. To investigate the melting point depression of Solvent-A, DSC plots of (1) pure Solvent-A, (2) organogel formulation with double Solvent-A (40w% Solvent-A) and (3) original formulation (25w% Solvent-A) were compared (Figure 4-10) Heating rate was 5°C/min for all of the DSC experiments.

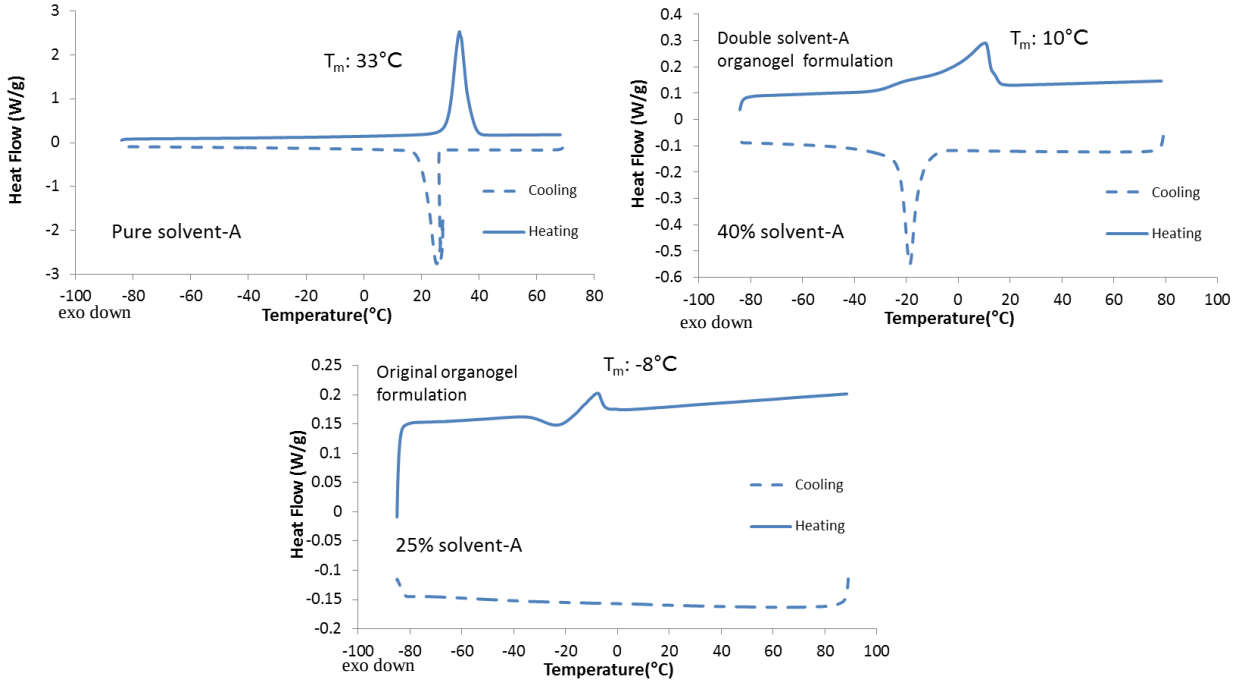

Figure 4-10: Melting point depression of Solvent-A

The melting point of Solvent-A depressed to 10°C and -8°C from 33°C for the double Solvent-A (40w%) and the original formulations(25w%) respectively. Intermolecular interactions such as hydrogen bonding between a polymer and a solvent may shift the melting point to lower temperatures[61].In addition, the original organogel formulation (25% Solvent-A) showed a cold crystallization behavior whereas the pure solvent and 40% Solvent-A formulation did not. At the lower concentrations of Solvent-A, solvent molecules were more kinetically hindered to crystallize upon cooling.

Effect of Curing Time and Network Structure

In Chapter-3, it was shown that, as the curing time increases, gel contents of the materials increase as a result of higher extent of reaction. Constitutive mechanical properties also increased with the curing time possibly due to the higher extent of reaction and the increased crosslink density. Therefore, it is expected that, at higher curing times, the gel network should be more confined which may affect the crystallization and melting behavior of Solvent-A in the organogel material. To investigate the effect of curing time on the thermal properties, DSC plots were obtained for the different curing times at 5°C/min heating/cooling rate. Figure 4-11 and 4-12 show the heating and cooling scans respectively.

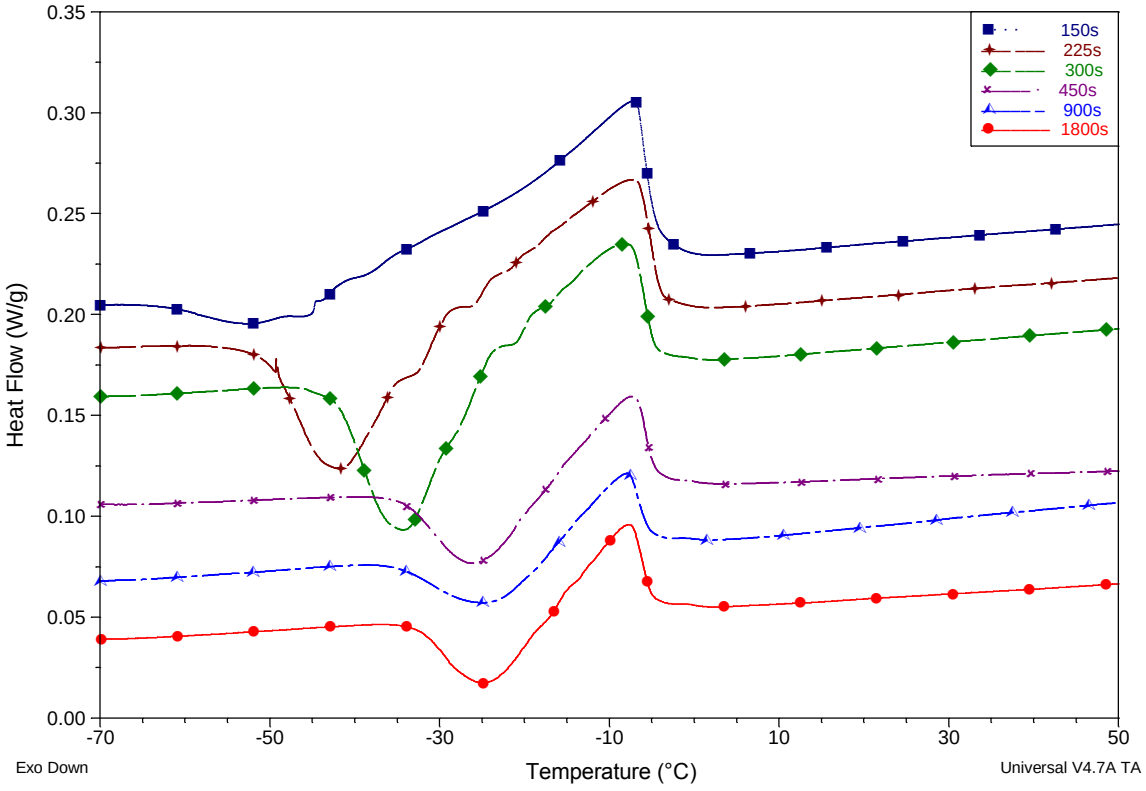

Figure 4-11: DSC heating scans of organogel materials cured for different times

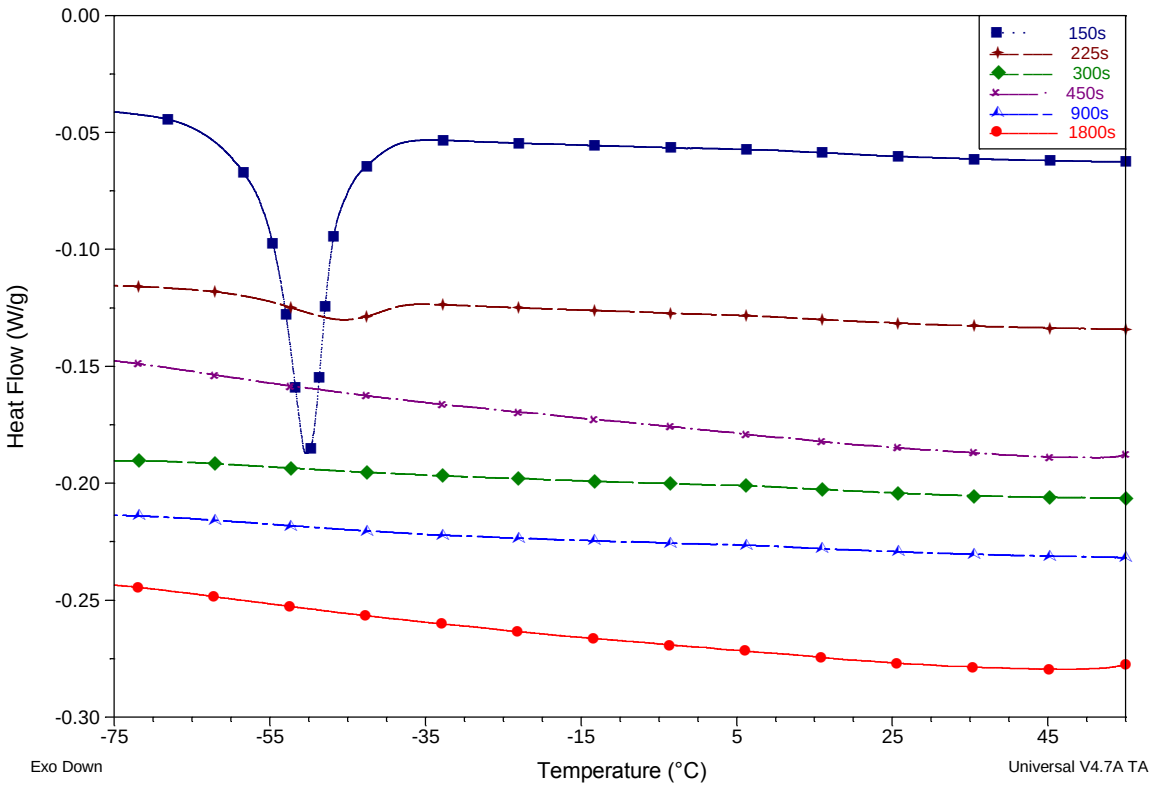

Figure 4-12: DSC cooling scans of organogel materials cured for different times

Except the 150s curing time, all the curing times showed only cold crystallization of the Solvent-A. Due to the system confinement and the mobility of the gel network, crystallization was kinetically inhibited during cooling. However, Solvent-A showed a different thermal behavior when it was in the 150s cured network. 150s cured material has the lowest gel content and the crosslink density. Therefore, at this curing time, solvent crystallization was not completely inhibited kinetically during the cooling. 150s curing time showed crystallization during both the heating and the cooling scans. Also, cold crystallization peaks of other curing times were much broader than the 150s curing time crystallization peak. Gel network mobility and heterogeneity in the distribution of network confinement[57] may result broadening of a crystallization peak.

Increasing confinement with the increasing curing time also showed a significant effect on the crystallization temperatures and the amount of crystallized Solvent-A molecules in the network. Table 4-1 summarizes the crystallization temperatures and the crystallization enthalpies.

Table 4-1: Crystallization temperatures and enthalpies of Solvent-A in organogels cured for different times

Curing time	Crystallization temperature, T_c(°C)	Crystallization enthalpy, ΔH(J/g)
150s	-50*	13.5*
225s	-42	11.4
300s	-34	9.3
450s	-26	4.1
900s	-25	3.6
1800s	-24	3.7
* Not cold crystallization		

As the curing time increased, the Solvent-A crystallization temperatures shifted to higher temperatures and crystallization enthalpy values decreased indicating that less solvent crystallize at higher curing times. During heating, at temperatures where the gel network mobility increases significantly due to a thermal transition (such as glass transition), cold crystallization process starts since the solvent molecule mobility increases accordingly [60]. At the lower curing times (225s and 300s), the gel network became mobile at lower temperatures during heating, therefore cold crystallization temperatures were at lower temperatures. Also, the crystallization enthalpies showed a direct relationship with the gel confinement. As the extent of reaction and the crosslink density increased with the curing time, the amount of the crystallized Solvent-A decreased since crystallization was hindered by the confined gel network. Baba et al. [68] previously showed a linear relationship between the gel content of an organogel and the solvent crystallization

enthalpy. A similar relationship was also obtained in this study (Figure 4-13). Therefore, it is shown that the gel network has significant effect on the solvent crystallization of an organogel.

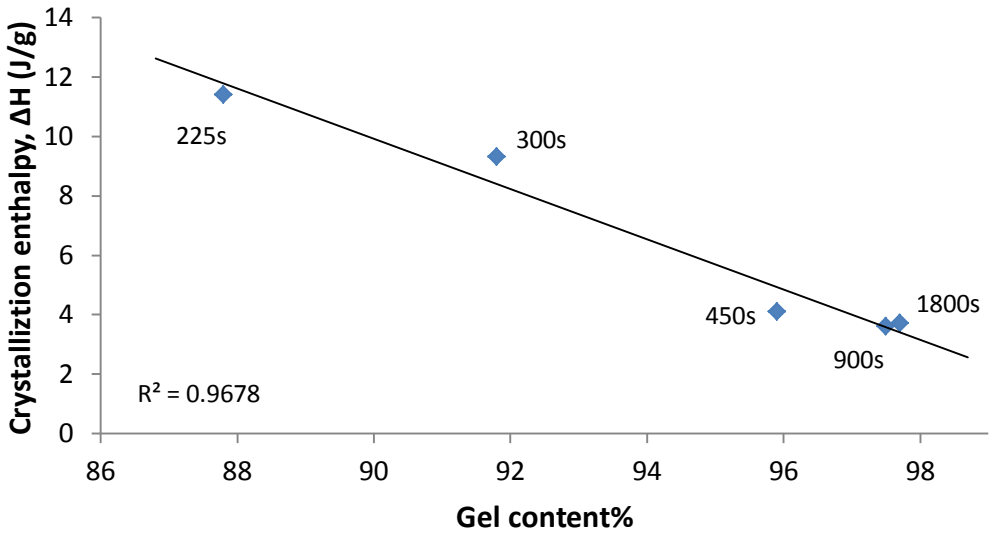

Figure 4-13: Effect of gel network on the solvent crystallization enthalpies

Changes in the gel network structure, thermal transition temperatures of the gel and the interactions between the polymer and the solvent can affect the thermal properties of the solvent in the organogel. Figure 4-13 shows that there is a linear relationship between the volume fraction of the gel varied by photo-curing time and the crystallization enthalpy (ΔH) of the solvent. Crystallization temperatures were also plotted as a function of the gel contents and another empirical linear relationship was observed between the crystallization temperatures and the gel content (Figure 4-14).

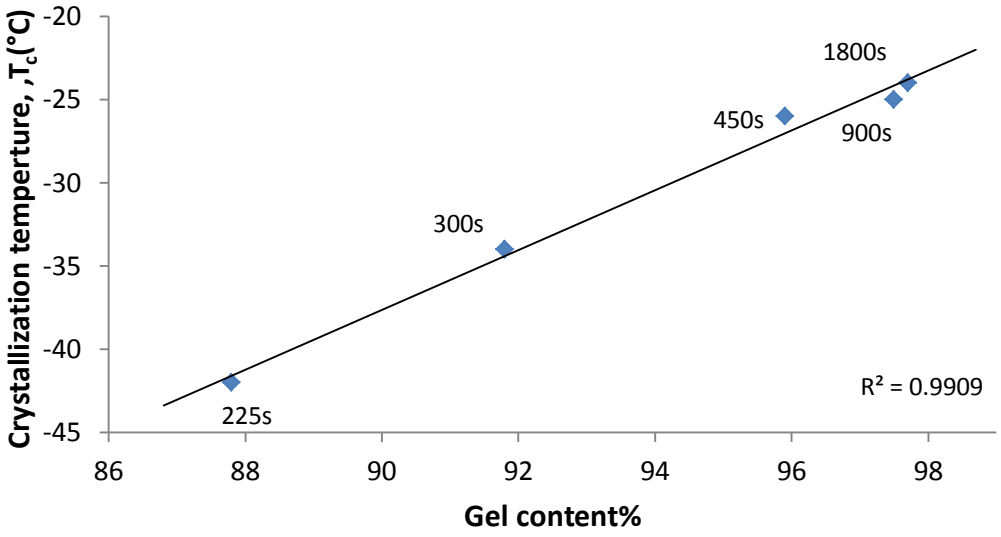

Figure 4-14: Effect of gel network on the solvent crystallization temperatures

In Chapter-3, it was shown that the curing time affects the gel content, constitutive mechanical properties and the fracture properties of the organogel. Generally, the changes after 450s curing time were insignificant since the material was almost fully cured after this curing time. Similarly, Solvent-A crystallization temperatures and melting enthalpies were not affected significantly by the curing time after 450s curing.

Effect of Solvent Crystallization on the Mechanical Properties

DMA plots of the organogels are shown on Figure 3-19. As the materials were heated through the leathery region, at some temperatures, shear modulus of the material showed an abnormal increase. The increase in the shear modulus in the leathery region was due to the solvent crystallization and in this section, the effect of the crystallization on the thermo-mechanical properties are discussed in detail.

Previously, thermal properties of the organogel without Solvent-A were characterized and there were no traces of crystallization (Figure 4-8 and 4-9). The formulation without Solvent-A has the

same solvent content however, it has only solvent-B which does not show any thermal phase changes in the DMA test temperature range. Figure 4-15 shows the comparison of the DMA heating scans of the original organogel formulation and the formulation without Solvent-A. Both of the materials were cured for 900s and the heating rate of the DMA experiment was 2°C/min.

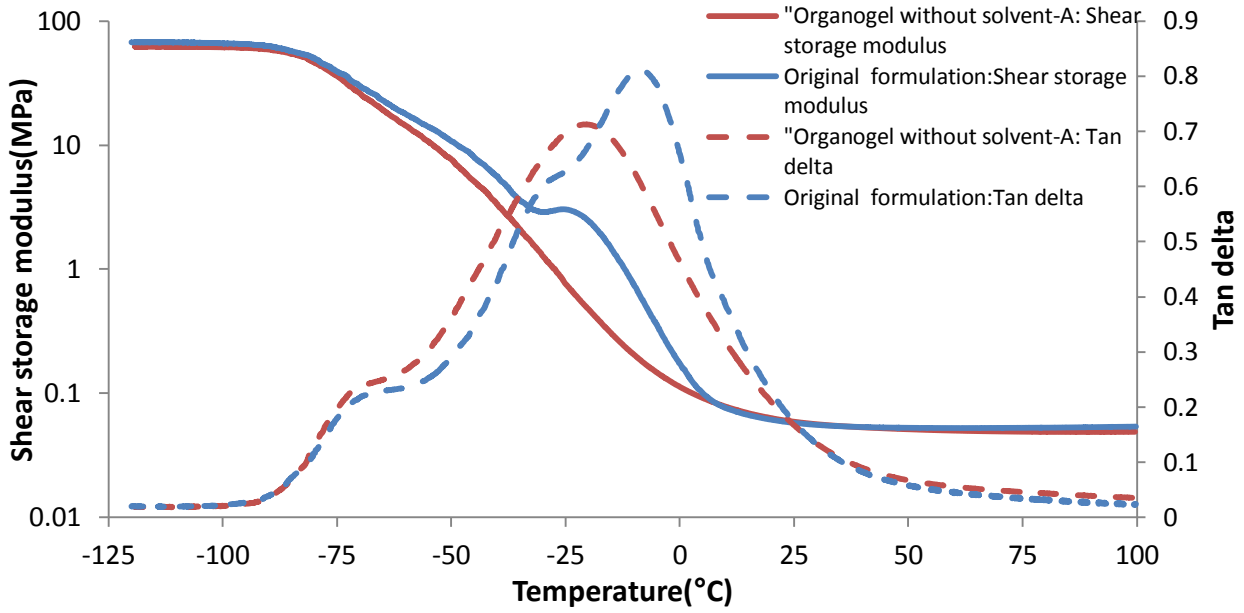

Figure 4-15: Effect of solvent-crystallization on thermomechanical properties

As the original organogel formulation was heated from the colder temperatures, at around -32°C, the decrease in the shear storage modulus stopped and a slight increase was observed until about -23°C. As previously discussed, Solvent-A in the organogel crystallizes when it is heated from colder temperatures. The observed increase in the shear storage modulus is due to the freezing of this component. The effect of crystallization on the shear modulus is significant when the original formulation is compared with the formulation without the Solvent-A (Figure 4-15). Honiball et al. showed that the unfrozen solvent can act as a plasticizer when they are present in an elastomer network and lowers the glass transition of the materials. However, when the solvent solidifies due to the crystallization, the plasticizer effect may be lost [75]. Increase in the shear

modulus on Figure 4-15 is due to the loss of plasticization effect of the Solvent-A due to the crystallization. Also, frozen solvent particles may reinforce the gel network, increasing the stiffness of the material.

Since both of the formulations have the same amount of solvent, the rubbery modulus and the glassy modulus of the materials were about the same. Also a shoulder was observed on the original formulation tan delta plot at a temperature where the crystallization was observed. This tan delta peak will be discussed in the following sections.

DSC plot on Figure 4-5 shows that Solvent-A in the organogel does not crystallize during the cooling scan however, crystallization occurs during the heating scan (cold crystallization). Figure 4-16 compares the cooling and heating DMA scans of the organogel.

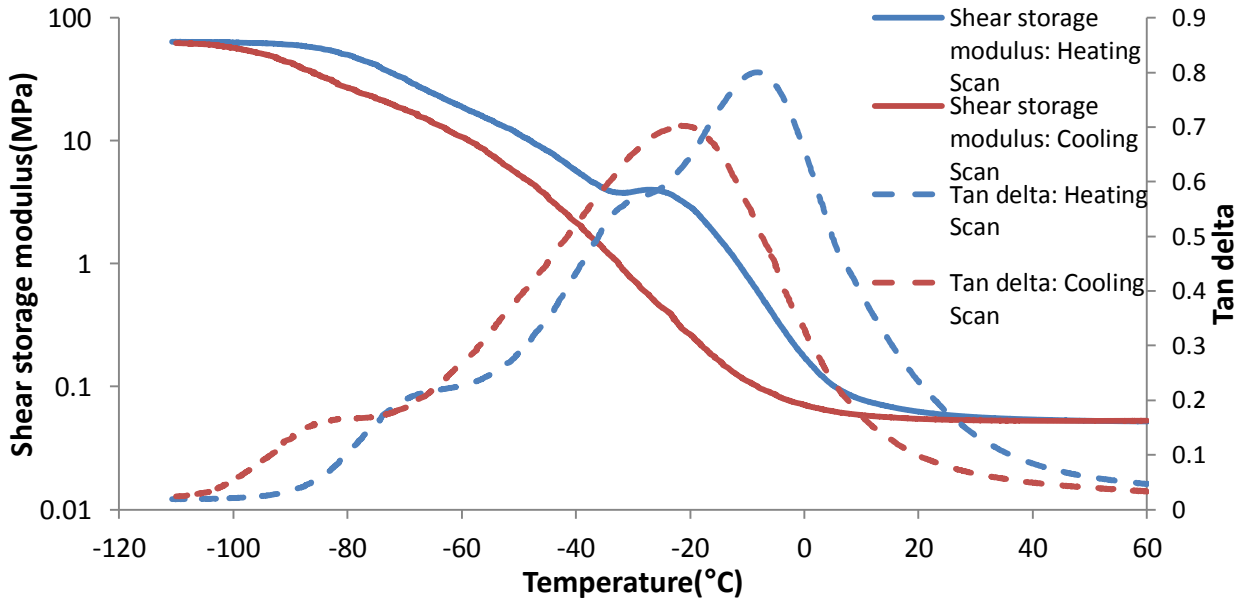

Figure 4-16: Comparison of the DMA heating and cooling scans

The modulus difference between the heating scan and the cooling scan at temperatures between -100°C and -35°C was possibly due to the thermal lag. At temperatures beyond -35°C, an increase

in shear modulus was observed due to the crystallization during the heating scan. However, this effect was not present on the cooling scan since there was no crystallization during cooling. An additional tan delta peak also appeared at the crystallization temperatures and this transition was not observed on the cooling plot. Also, the heating scan α transition tan delta peak was at -9°C whereas the cooling scan α transition peak was at -20°C. As previously discussed, the solvent losses its plasticizer effect when it solidifies. Therefore, during heating, the gel network became stiffer than the gel network during cooling. Since more energy is required for the relaxation of stiffer chains, the transition was observed at higher temperatures on the heating scan.

The dynamic mechanical properties of viscoelastic materials are sensitive to both the temperature and the frequency of deformation since polymer chain mobility is affected by both of the factors. Storage moduli and thermal transitions (tan delta peak max) of the materials usually shift to higher temperatures with the increasing frequency. On Figure 4-15 and 4-16, a tan delta peak was observed at the temperatures where the crystallization occurs. First-order transitions such as melting and crystallization does not show frequency dependence unlike the second-order transitions such as glass transition[76, 77]. To investigate the effect of frequency of deformation, DMA heating plots were obtained at different frequencies (Figure 4-17 and Figure 4-18).

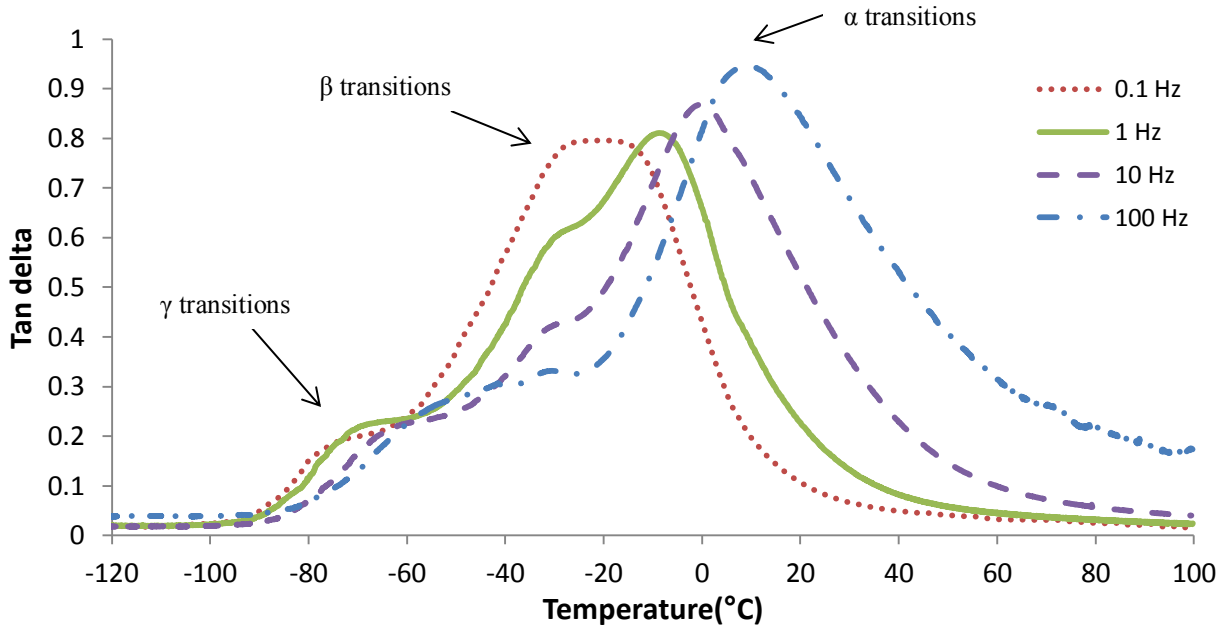

Figure 4-17: Effect of frequencies of deformation, tan delta heating scans

Figure 4-17 shows that the γ and α transitions shift to higher temperatures with the increasing deformation frequency. However, the β transition was not affected by the changes in the frequency. The summary of the thermal transition temperatures are shown in Table 4-2. Solvent molecules in the organogel increase the free volume in the system. High frequency dependence of the α transition temperatures can be correlated with high available free volume.

Table 4-2: Tan delta transition temperatures at different frequencies

Frequency (Hz)	**0.1**	**1**	**10**	**100**
α transition tempearature (°C)	-20	-9	0	9
β transition tempearature (°C)	-29	-29	-30	-31
γ transition tempearature (°C)	-77	-71	-63	-57

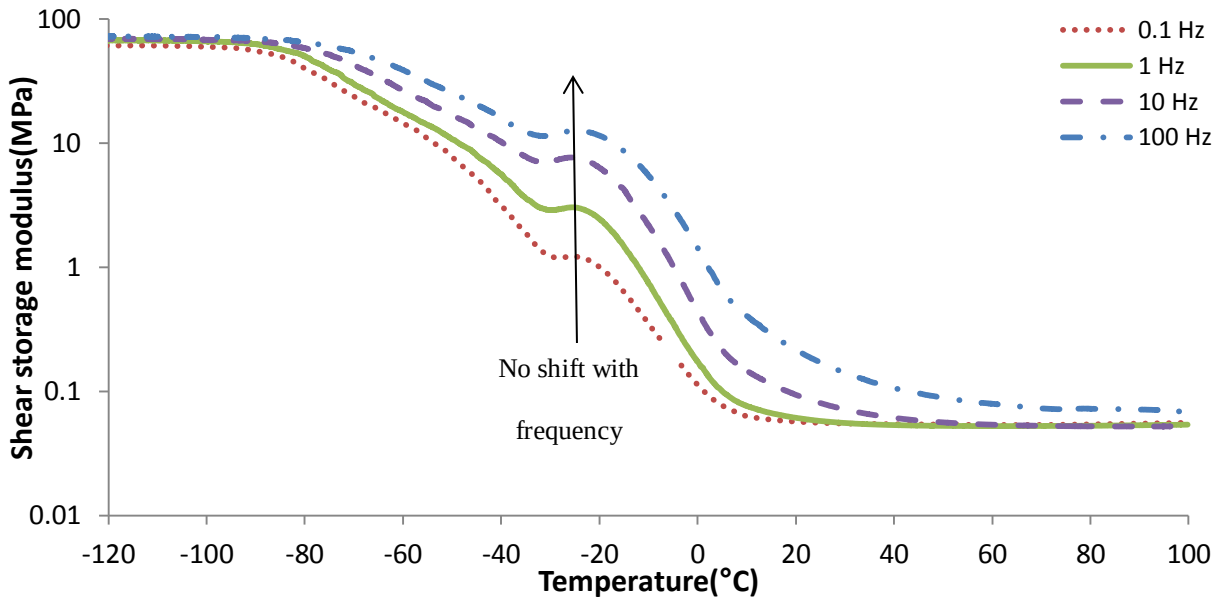

Figure 4-18: Effect of frequencies of deformation, shear storage modulus heating scans

The storage moduli of viscoelastic materials shifted to higher values with the increase in frequency. However, in the temperature range of -32°C to -23°C, there was no shift with the frequency since the crystallization was not affected by the frequency of deformation of the DMA experiments. Therefore, it is concluded that the β transition at -30°C is a frequency independent transition which occurs as a result of the cold crystallization of the material.

Effect of Heating Rate and Minimum Cooling Temperatures

In order to investigate the effect of heating rate, DSC and DMA tests were performed at different heating rates. The DSC heating rates were 1,2,4,8 and 16°C/min and DMA heating rates were 1,2 and 4°C/min. Since, larger specimens are used for the DMA experiments, thermal lag is a problem therefore the maximum selected heating rate was 4°C/min. Figure 4-19 and Figure 4-20 shows the effect of heating rate on the crystallization of Solvent-A and its effects on the thermo-mechanical properties.

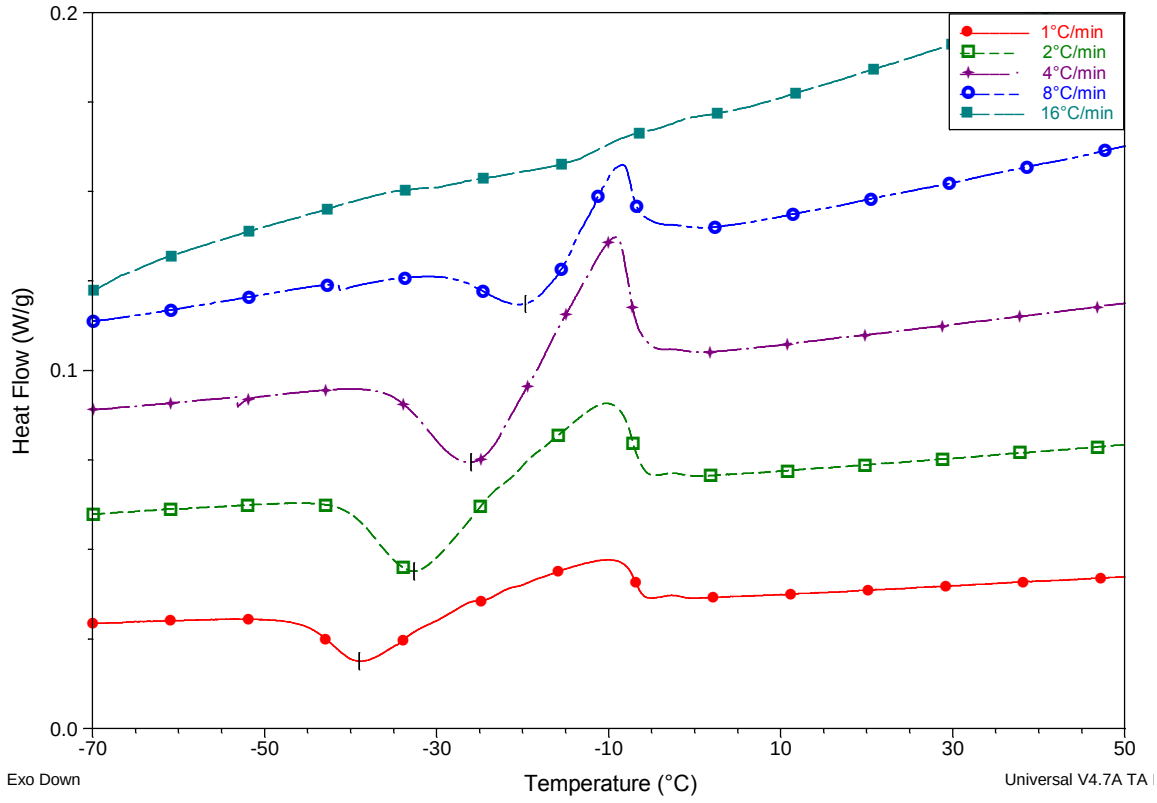

Figure 4-19: Effect of heating rate on crystallization of Solvent-A

DSC crystallization enthalpies and crystallization temperatures were obtained from Figure-4-19. Using the crystallization enthalpy of the pure Solvent-A (165 J/g), the percentage of the crystallized Solvent-A in the organogel material was obtained. Table 4-3 summarizes the effect of heating rate on crystallization of Solvent-A.

Table 4-3: Effect of heating rate on crystallization of Solvent-A

Heating rate (°C/min)	**Crystallization temperature (°C/min)**	**ΔH(J/g)**	**% crystallized Solvent-A in the organogel**
1	-39	8.6	20.9
2	-33	6.6	16
4	-26	3.6	8.7
8	-20	0.9	2.2
16	-	-	-

As the heating rate increased, the crystallization temperatures of Solvent-A shifted to higher temperatures. However, the crystallization enthalpy decreased with the increasing heating rate. Therefore, lower percentages of Solvent-A crystallized at the higher rates. Cold crystallization depends on the segmental mobility of the chains in the gel network. As the heating rate increases, thermal transition temperatures shift towards to higher temperatures. Therefore higher cold crystallization temperatures were observed at the higher heating rates. Since crystallization is a kinetic phenomenon, the amount of the crystallized Solvent-A decreased with the increasing heating rate. At 16°C/min heating rate, crystallization was not observed by DSC.

Previously, the effect of crystallization on the mechanical properties of the organogel was discussed in detail. In this section, the effect of subsequent changes in the crystallization behavior as a result of changing heating rate on the thermo-mechanical properties is discussed. Figure 4-20 shows the DMA plots obtained at different heating rates.

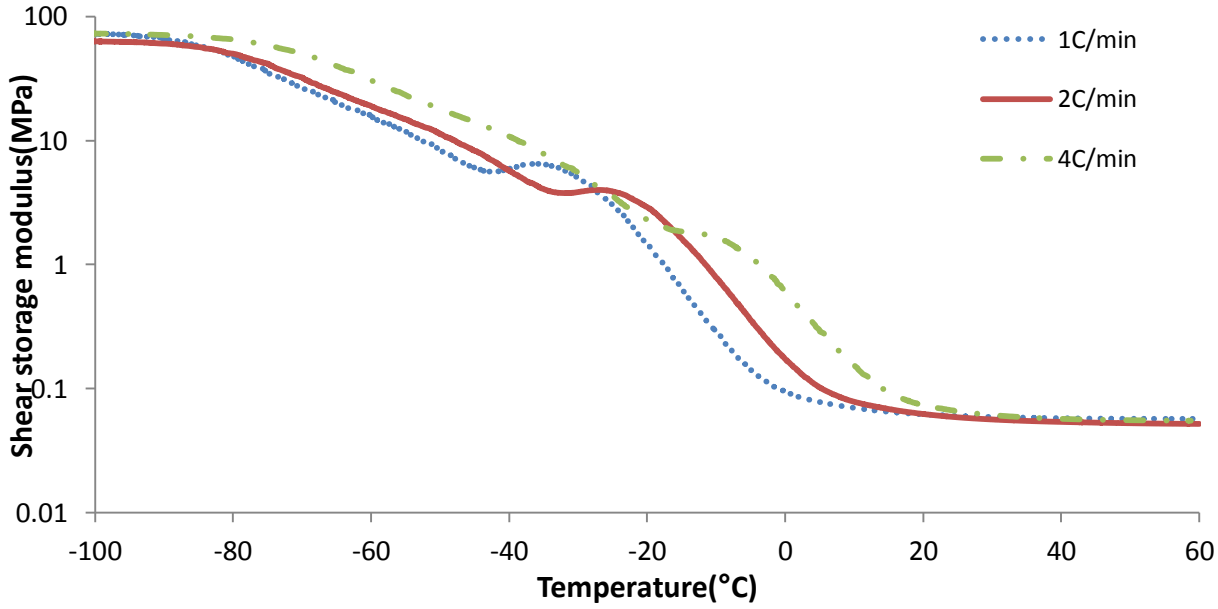

Figure 4-20: Effect of heating rate on the thermo-mechanical properties

DSC results showed that the crystallization temperatures shift to higher temperatures at higher heating rates. Figure 4-20 indicates that the onset of modulus increase due to crystallization of Solvent-A increases with the increasing heating rating.

Table 4-4: Comparison of crystallization temperatures and the onset of modulus increase due to crystallization

Heating rate (°C/min)	DSC crystallization temperature (°C)	DMA onset of modulus increase (°C)
1	-39	-43
2	-33	-33
4	-26	-17

Table 4-4 shows that the onset of modulus increase temperatures observed by the DMA is relevant with the DSC results. The difference between the temperatures at 4°C/min heating rate was probably caused by the thermal lag at high heating rates.

The mechanical properties of the organogel material can be altered by freezing the Solvent-A which loses its plasticizer effect in the solid state. Since Solvent-A showed a cold crystallization behavior, in order to induce the crystal formation, the material should be cooled down to a certain temperature and heated back to higher temperatures. In this section, the effects of minimum cooling temperature on the crystallization behavior and thermo-mechanical properties are studied. The minimum cooling temperatures used for the DSC and DMA studies were in the range of -25°C and -60°C. Figure 4-24 shows the DSC plots of 900s cured specimens which were heated from different minimum temperatures at 5°C/min heating rate.

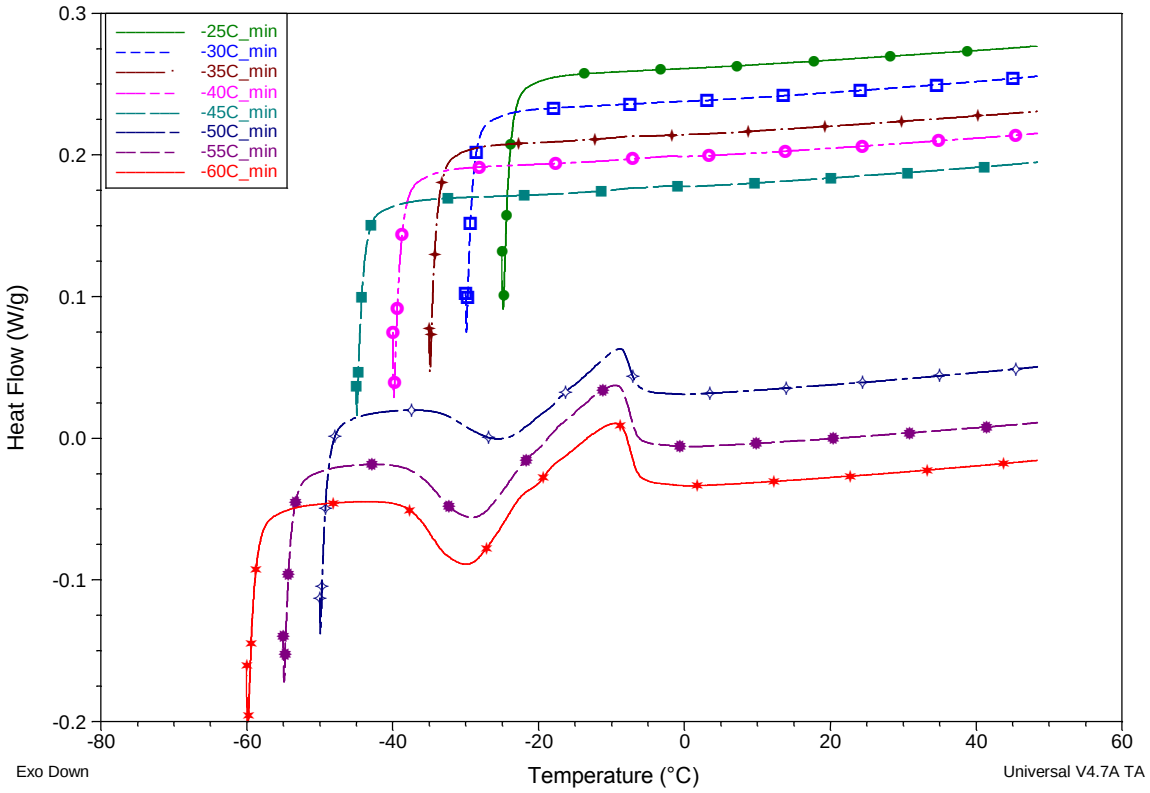

Figure 4-21: Effect of minimum cooling temperatures

Figure 4-21 shows that Solvent-A does not crystallize when the material is heated from -45°C or above. However, when the organogel was heated from -50°C or below, crystallization and melting peaks were observed. Therefore, in order to induce the crystal formation and in order to increase the modulus of the material by solidifying the solvent, the material should be cooled down to minimum temperature of -50°C. It should be noted that, the amount of freezing Solvent-A increased as the minimum cooling temperatures are decreased (Table 4-5)

Table 4-5: Effect of minimum cooling temperature on Solvent-A crystallization enthalpies at 5°C/min heating rate

Minimum cooling temperature(°C)	Crystallization enthalpy(J/g)
-50	3
-55	5.1
-60	6.3

The effect of minimum cooling temperatures on the thermo-mechanical properties were studied by DMA. At a given range of -20 to -60°C, an increase in the storage modulus due to the solvent solidification was only observed with the -50 and -60°C minimum cooling temperatures (Figure 4-22). These temperatures were consistent with the DSC experiments shown in Figure 4-22.

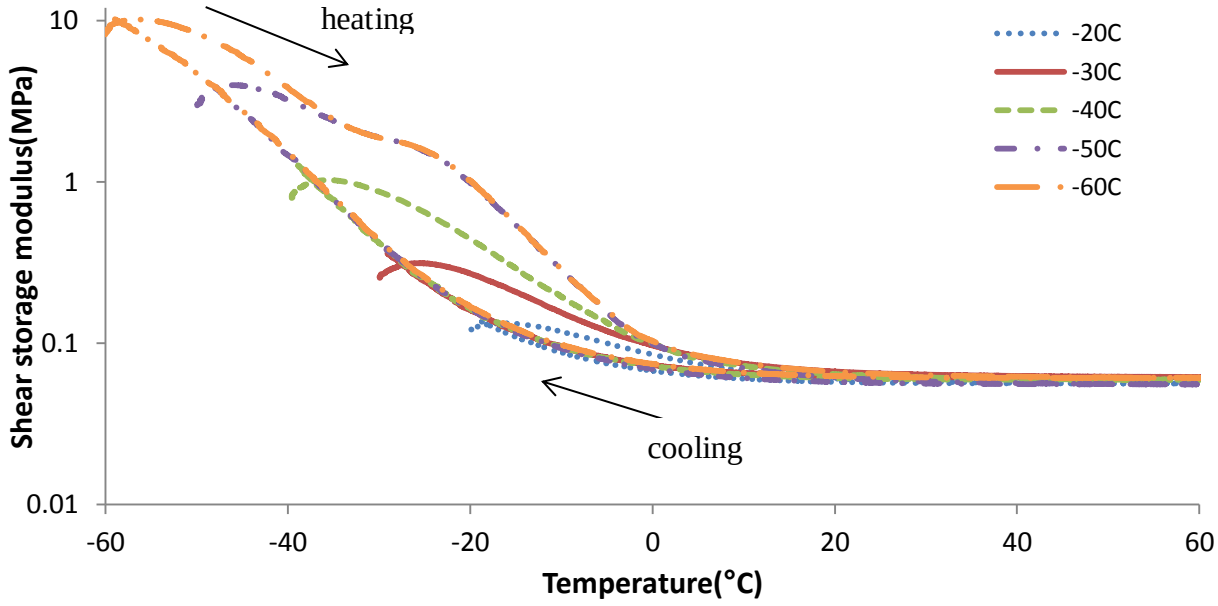

Figure 4-22: Effect of minimum heating temperature on thermo-mechanical properties

Conclusions

In this chapter, crystallization and melting behavior of Solvent-A and its subsequent effects on the thermo-mechanical properties were studied in detail. Solvent-A showed a cold crystallization behavior since the crystallization was kinetically hindered during cooling due to the reduced network mobility. By comparing the original formulation and the formulation without Solvent-A, it was confirmed that, the crystallization and melting observed by DSC and thermal optical microscopy are due to the phase changes of Solvent-A in the organogel. Additionally, two melting transitions were observed at around -30°C and -10°C by thermal optical microscopy and this behavior was also confirmed by MDSC. The two melting transitions

were correlated with the different types of interactions of Solvent-A and the gel network as well as the heterogeneity of the organogel network. However, the amount of the component which melted at around -10°C (second melting) was much larger than the first melting component. Therefore, in this study, that transition and its effects on the mechanical properties were studied in detail. The melting point of the Solvent-A depressed to -8°C from 33°C when it was present in the organogel network. Depression in the melting point was correlated with the intermolecular interactions between the solvent and the polymer network.

The effect of curing time on the mechanical, viscoelastic and fracture properties of the organogel was studied in Chapter-3. In this chapter, it was shown that, curing time also significantly affects the crystallization behavior of Solvent-A. As the curing time increased, the crystallization temperatures of Solvent-A shifted to higher temperatures since the gel network became more confined due to the higher crosslink density and the higher extent of reaction. Also, less Solvent-A crystallized at higher curing times. A linear empirical relationship was showed between the solvent crystallization temperatures/crystallization enthalpies and the gel contents for the materials cured for different times.

In the gel network, Solvent-A acts as a plasticizer and lowers the stiffness of the material. However, when it was solidified by cold crystallization, it did not act as a plasticizer anymore and the modulus of the material increased. DMA plots showed an increase in the shear storage modulus at the crystallization temperatures. However, the increase was only on the heating scans but not on the cooling scans since Solvent-A crystallizes only during heating from colder temperatures. Also, a frequency independent tan delta peak associated with the crystallization was observed. Since crystallization is a first order transition, the tan delta peak did not shift to higher temperatures at higher frequencies.

Finally, the effect of processing parameters such as the heating rate and the minimum cooling temperatures on the crystallization and the thermo-mechanical properties were studied. As the heating rate increased, the crystallization temperatures shifted to higher temperatures and the amount of the crystallized Solvent-A molecules decreased. DMA tests also performed at different heating rates and the onset of modulus increase temperatures were relevant with the crystallization temperatures observed by the DSC. Additionally, crystallization of Solvent-A was observed only when it was heated from temperatures of -50°C and below. Similarly, the effect of crystallization on the thermomechanical properties was apparent when the specimens were heated from -50°C and below.

Chapter 5 : Conclusions

Conclusions

In this chapter, key observations and conclusions are summarized. In Chapter-2, silicone semi-IPN organogel material preparation for the bulk and adhesive fracture testing was explained. Chapter-3 was focused on the effect of curing time on the constitutive and fracture properties of the organogel. Curing time is an important parameter which has significant effect on the properties of the material. The important conclusions from Chapter-3 were:

- Gel contents of the organogels increased with the increasing curing time due to the higher extents of reactions.
- Uniaxial tensile behavior of the organogels was characterized by neo-Hookean material model. Significant increase in the shear modulus of the organogels was observed with the increasing curing time.
- Increase in the mechanical properties was also observed by DMA. Shear storage modulus in the rubbery and leathery regions were higher at higher curing times due to the higher extent of reaction and crosslink density.
- Because of the reduced chain mobility at higher curing times, thermal transition temperatures shifted to higher temperatures.
- The shape of the gel content, shear modulus and glass transition temperature vs. curing time plots were very similar to one another (Figures 3-16, 3-18 and 3-21). The changes in the material properties were insignificant after 450s curing time since the material was almost fully cured at this curing time.

- Cohesive fracture properties were characterized by constrained fracture tests. Higher moduli at the higher curing times resulted greater strain energy release rates. However, due to the increasing crosslink density, organogels became more brittle and crack propagation rates increased.
- Adhesive fracture properties between the organogel and a cyclo-olefin polymer were characterized by wedge tests. The SERR values were found to be the same for all the curing times except the 150s curing time. At this curing time, due to the higher viscoelastic dissipation, SERR values were higher at given crack propagation values.

In Chapter-4, thermal properties of Solvent-A in the organogel studied in detail. DSC, thermal optical microscopy and DMA were used to characterize the phase change of the solvent and its effects on the mechanical properties. From the thermal properties of Solvent-A, important findings were obtained about the properties of the gel network. The key findings of these studies were:

- Crystallization of Solvent-A was confirmed by DSC and thermal optical microscopy through the characterization of the formulations with different Solvent-A contents.
- Solvent-A crystallized during the heating scans but not during cooling scans since the crystallization was kinetically hindered during the cooling scans (cold crystallization).
- Solvent-A showed two different melting transitions possibly due to the different types of interactions and network mesh sizes. However, the amount of the second melting component (at around -8°C) was much larger than the first melting component (at around -29°C).

- The melting point of Solvent-A shifted to -8°C from 33°C when it was in the gel network. The melting point depression was possibly due to the intermolecular interactions between the solvent and the gel network.
- Increasing curing time made the gel network stiffer which shifted the crystallization temperatures to higher temperatures and lowered the amount of the crystallized Solvent-A in the organogel.
- A linear relationship was observed between the crystallization temperatures/enthalpies and the gel contents of the organogels cured for different curing times.
- When Solvent-A solidified as a result of the cold crystallization, stiffness of the organogel material increased since the solvent did not act as a plasticizer in the network, in the solid form. Another reason for the increase in the mechanical properties would be the reinforcing effect of the solid solvent particles.
- A tan delta peak associated with the crystallization of Solvent-A was observed on the DMA heating scans. Since crystallization is a first order transition, the tan delta peak was frequency independent.
- Increasing heating rate shifted the crystallization temperatures to higher values and decreased the amount of crystallized Solvent-A. The onsets of modulus increase temperatures from DMA were relevant with the crystallization temperatures from the DSC experiments.
- In order to induce crystallization at 5°C/min heating rate, organogels should be heated from at most -50°C. Within the range of -50°C to -60°C, as the minimum temperature was lowered, the amount of the crystallized Solvent-A increased. Similar results were also obtained by DMA on the stiffness increase due to the solvent crystallization.

Future Work

This study provided important insights on some of the properties and manufacturing variables of the organogel material. However, there are some important areas to understand the properties of the material and its components, as well as the manufacturing parameters of this type of materials. The prospective future work includes:

- Curing the organogel at different temperatures and characterizing the constitutive and fracture properties of resulting materials.
- Characterizing cohesive and adhesive fracture properties after thermal processing is applied to solidify Solvent-A.
- Implementing digital image correlation and finite element analysis methods to fully understand the changes in the viscoelastic properties of different organogels which are fabricated using different manufacturing parameters such as curing time.
- Analyzing curing shrinkage and thermal shrinkage of the organogel and their subsequent effects on the fracture of the material.
- Characterizing the thermal properties of Solvent-A in different gel systems for further understanding of cold crystallization behavior and interactions between the solvent and the gel network.

References

1. Sperling, L.H., *Interpenetrating Networks and Related Materials,*1981, New York: Plenum Press.
2. Wang, J., F. Liu, and J. Wei, *Hydrophilic silicone hydrogels with interpenetrating network structure for extended delivery of ophthalmic drugs.* Polymers for Advanced Technologies, 2011: p. n/a-n/a.
3. Edmund Co and A.G. Marangoni, *Structured Organogels Based on Vegetable Oils and Surfactants— Structures, Characteristics and Applications*, in *Nanotechnologies for Solubilization and Delivery in Foods, Cosmetics and Pharmaceuticals*, Nissim Garti and I. Amar-Yuli, Editors. 2011, DEStech Publications: Lanchester, PA.
4. Decker, C., *Kinetic Study and New Applications of UV Radiation Curing.* Macromol. Rapid Commun., 2002. **23**(18): p. 1067-1093.
5. Wang, J. and X. Li, *Preparation and characterization of interpenetrating polymer network silicone hydrogels with high oxygen permeability.* Journal of Applied Polymer Science, 2010. **116**(5): p. 2749-2757.
6. Wang, J. and X. Li, *Interpenetrating polymer network hydrogels based on silicone and poly(2-methacryloyloxyethyl phosphorylcholine).* Polymers for Advanced Technologies, 2011. **22**(12): p. 2091-2095.
7. Wang, J. and F. Liu, *UV-curing of simultaneous interpenetrating network silicone hydrogels with hydrophilic surface.* Polymer Bulletin, 2012.
8. Shimizu, T., et al., *Super-hydrophilic silicone hydrogels with interpenetrating poly(2-methacryloyloxyethyl phosphorylcholine) networks.* Biomaterials, 2010. **31**(12): p. 3274-3280.
9. Liu, L. and H. Sheardown, *Glucose permeable poly (dimethyl siloxane) poly (N-isopropyl acrylamide) interpenetrating networks as ophthalmic biomaterials.* Biomaterials, 2005. **36**(3): p. 233-244.
10. Kronberg, B. and A. Hillerstro, *A Two-Step Method for the Synthesis of a Hydrophilic PDMS Interpenetrating Polymer Network.* Journal ofApplied Polymer Science, 2008. **110**: p. 3059–3067 (2008).
11. Ramaraj, B. and G. Radhakrishnan, *Modification of the dynamic swelling behaviour of poly(2-hydroxyethyl methacrylate) hydrogels in water through interpenetrating polymer networks (IPNs).* Polymer, 1994. **35**(10): p. 2167-2173.
12. Pavlyuchenko, V.N., et al., *New silicone hydrogels based on interpenetrating polymer networks comprising polysiloxane and poly(vinyl alcohol) networks.* Polymers for Advanced Technologies, 2009. **20**(4): p. 367-377.
13. Chekina, N.A., et al., *A new polymeric silicone hydrogel for medical applications: synthesis and properties.* Polymers for Advanced Technologies, 2006. **17**(11-12): p. 872-877.
14. Abbasi, F., H. Mirzadeh, and A.A. Katbab, *Sequential interpenetrating polymer networks of poly(2-hydroxyethyl methacrylate) and polydimethylsiloxane.* Journal of Applied Polymer Science, 2002. **85**(9): p. 1825-1831.
15. Abbasi, F., H. Mirzadeh, and A.A. Katbab, *Comparison of Viscoelastic Properties of Polydimethylsiloxane/Poly(2-Hydroxyethyl Methacrylate) IPNs with Their Physical Blends.* Journal of Applied Polymer Science, 2002. **86**(14): p. 3480-3485.

16. Abbasi, F., H. Mirzadeh, and M. Simjoo, *Hydrophilic interpenetrating polymer networks of poly (dimethyl siloxane)(PDMS) as biomaterial for cochlear implants.* Journal of Biomaterials Science, Polymer Edition, 2006. **17**(3): p. 341–355.
17. Murray, K.V., *Characterization of the Interfacial Fracture of Solvated Semi-Interpenetrating Polymer Network (S-IPN) Silicone Hydrogels with a Cyclo-Olefin Polymer (COP)* in *Engineering Mechanics* 2011, Virginia Polytechnic Institute and State University Blacksburg, VA.
18. Tizard, G.A., *Characterization of the Viscoelastic Fracture of Solvated Semi-Interpenetrating Polymer Network (S-IPN) Silicone Hydrogels* in *Engineering Mechanics* 2010, Virginia Polytechnic Institute and State University: Blacksburg, VA
19. Pappas, S.P., *Radiation Curing: Science and Technology*1992, New York: Plenum Press.
20. Ranby, B., B. Qu, and W. Shi, *Polymeric Materials Encyclopedia*, in *Polymeric Materials Encyclopedia*, J.C. Salamone, Editor 1996, CRC Press: Florida.
21. Dolez, P., M. Marek, and B.J. Love, *Photopolymerizable Acrylic Resin : Effect of Curing Time and Temperature.* Journal of Applied Science, 2001. **82**: p. 546-554.
22. Emami, N. and K.J.-M. Söderholm, *How light irradiance and curing time affect monomer conversion in light-cured resin composites.* European journal of oral sciences, 2003. **111**(6): p. 536-542.
23. Cadenaro, M., et al., *Effect of adhesive hydrophilicity and curing time on the permeability of resins bonded to water vs. ethanol-saturated acid-etched dentin.* Dental Materials, 2009. **25**(1): p. 39-47.
24. Baek, C.-J., et al., *The Effects of Light Intensity and Light-curing Time on the Degree of Polymerization of Dental Composite Resins.* Dental Materials Journal, 2008. **27**(4): p. 523-533.
25. Mohsen, N.M., R.G. Craig, and F.E. Filisko, *Effects of curing time and filler concentration on curing and postcuring of urethane dimethacrylate composites: a microcalorimetric study.* Journal of biomedical materials research, 1998. **40**(2): p. 224-232.
26. Vennemann, N., K. Bokamp, and D. Broker. *Crosslink density of dynamically vulcanized polyolefin blends (TPV) based on EPDM/PP*. in *Thermoplastic Elastomers*. 2006. Munich, Germany: iSmithers Rapra Publishing.
27. Pradas, M.M., et al., *Interaction between water and polymer chains in poly(hydroxyethyl acrylate) hydrogels.* Colloid & Polymer Science, 2001. **279**(4): p. 323-330.
28. Hamed, G.R., *Materials and Compounds*, in *Engineering With Rubber: How to Design Rubber Components*, A.N. Gent, Editor 2001, Hanser Verlag: Ohio.
29. Kim, J., A. Conway, and A. Chauhan, *Extended delivery of ophthalmic drugs by silicone hydrogel contact lenses.* Biomaterials, 2008. **29**(14): p. 2259-2269.
30. Meyers, M.A. and K.K. Chawla, *Mechanical Behavior of Materials*1999, United Kingdom: Cambridge University Press.
31. Brinson, H.F. and L.C. Brinson, *Polymer Engineering Science and Viscoelasticity*2008, New York: Springer.
32. Sanabria-DeLong, N., A.J. Crosby, and G.N. Tew, *Photo-Cross-Linked PLA-PEO-PLA Hydrogels from Self-Assembled Physical Networks: Mechanical Properties and Influence of Assumed Constitutive Relationships.* Biomacromolecules, 2008. **9**(10): p. 2784-2791.
33. Seitz, M.E., et al., *Fracture and large strain behavior of self-assembled triblock copolymer gels.* Soft Matter, 2009. **5**: p. 447-456.

34. Creton, C., G. Hu, and F. Deplace, *Large-Strain Mechanical Behavior of Model Block Copolymer Adhesives.* Macromolecules, 2009. **42**: p. 7605-7615.
35. Tew, G.N. and S.R. Bhatia, *PLA–PEO–PLA Hydrogels and Their Mechanical Properties*, in *Engineering Biomaterials for Regenerative Medicine*, S.K. Bhatia, Editor 2012, Springer: New York.
36. McCrum, N.G., C.P. Buckley, and C.B. Bucknall, *Principles of Polymer Engineering*. 2 ed2007, New York: Oxford University Press.
37. Rivlin, R.S. and A.G. Thomas, *Rupture of rubber. I. Characteristic energy for tearing.* Journal of Polymer Science, 1953. **10**(3): p. 291-318.
38. Lin, W.C., et al., *Large Strain and Fracture Properties of Poly(dimethylacrylamide)/Silica Hybrid Hydrogels.* Macromolecules, 2010. **43**(5): p. 2554-2563.
39. Gent, A.N., *A New Constitutive Relation for Rubber.* Rubber Chemistry and Technology, 1966. **69**(1): p. 59-61.
40. Griffith, A.A., *The Phenomena of Rupture and Flow in Solids.* Philosophical Transactions of the Royal Society of London, 1921. **A221**: p. 163-198.
41. Ward, I.M. and D.W Hadlty, *An Introduction to the Mechanical Properties of Solid Polymers*1993, United Kingdom: John Wiley & Sons.
42. Creton, C., et al., *Adhesion and Fracture of Interfaces Between Immiscible Polymers: from the Molecular to the Continuum Scale*, in *Advances in Polymer Science*, A. Abe, Albertsson, A.-C., Dusek, K., Genzer, J., Jeu, W.H. de, Kobayashi, S., Lee, K.-S., Leibler, L., Long, T.E., Manners, I., Möller, M., Terentjev, E.M., Vicent, M.J., Voit, B., Wiesner, U., Editor 2002, Springer Berlin / Heidelberg. p. 53-136.
43. Creton, C., et al. *Fracture and Adhesion of Soft Viscoelastic Materials and Gels* in *13th International Conference on Deformation Yield and Fracture of Polymers*. 2006. Kerkrade, The Netherlands.
44. Lake, G.J. and A.G. Thomas, *The Strength of Highly Elastic Materials.* Proceedings of the Royal Society of London. Series A. Mathematical and Physical Sciences, 1967. **300**(1460): p. 108-119.
45. Karger-Kocsis, J., *Fracture Mechanical Behavior of Thermoplastic Polymers as a Function of Molecular and Supramolecular Variables*, in *The Application of Fracture Mechanics to Polymers, Adhesives and Composites*, D.R. Moore, Editor 2004, Elsevier: United Kingdom.
46. Gent, A.N. and S.M. Lai, *Interfacial bonding, energy dissipation, and adhesion.* Journal of Polymer Science Part B: Polymer Physics, 1994. **32**(8): p. 1543-1555.
47. Josse, G., et al., *Measuring interfacial adhesion between a soft viscoelastic layer and a rigid surface using a probe method.* The Journal of Adhesion, 2004. **80**(1-2): p. 87-118.
48. Adams, R.D., et al., *The relative merits of the Boeing wedge test and the double cantilever beam test for assessing the durability of adhesively bonded joints, with particular reference to the use of fracture mechanics.* International Journal of Adhesion and Adhesives, 2009. **29**(6): p. 609-620.
49. ASTM, *Standart Test Method for Adhesive-Bonded Surface Durability of Aluminum*, 2003, ASTM International: West Conshohockeen, PA.
50. Ghatak, A., L. Mahadevan, and M.K. Chaudhury, *Measuring the Work of Adhesion between a Soft Confined Film and a Flexible Plate.* Langmuir, 2005. **21**(4): p. 1277-1281.

51. Dillard, D.A., *Bending of Plates on Thin Elastomeric Foundations.* Journal of Applied Mechanics, 1989. **56**(2): p. 382-386.
52. Tobolsky, A.V., *Viscoelastic Properties of Polymers*, in *Polymer Science and Materials*, A.V.T.H.F. Mark, Editor 1971, John Wiley & Sons USA.
53. Stutz, H., K.H. Illers, and J. Mertes, *A generalized theory for the glass transition temperature of crosslinked and uncrosslinked polymers.* Journal of Polymer Science Part B: Polymer Physics, 1990. **28**(9): p. 1483-1498.
54. S. Sahoo, et al., *Organogels: Properties and Applications in drug delivery.* Designed Monomers and Polymers, 2011. **14**(95-108).
55. Vintiloiu, A. and J.-C. Leroux, *Organogels and their use in drug delivery — A review.* Journal of Controlled Release, 2008. **125**(3): p. 179-192.
56. Markovic, N. and N.K. Dutta, *Physical organogels: mechanism and kinetics of evaporation of the solvents entrapped within network scaffolding.* Thermochimica Acta, 2005. **427**(1–2): p. 207-219.
57. Markovic, N., M. Ginic-Markovic, and N.K. Dutta, *Mechanism of solvent entrapment within the network scaffolding in organogels: thermodynamic and kinetic investigations.* Polymer International, 2003. **52**(7): p. 1095-1107.
58. Markovic, N., M. Ginic-Markovic, and N.K. Dutta, *Benzene physical and chemical organogels: Effect of network scaffolding on the thermodynamic behavior of entrapped solvent molecules.* Journal of Applied Polymer Science, 2004. **94**(3): p. 1253-1264.
59. de Jong, J., B.L. Feringa, and J. van Esch, *Responsive Molecular Gels*, in *Molecular Gels: Materials with Self-Assembled Fibrillar Networks*, R.G. Weiss and P. Terech, Editors. 2006, Springer: Netherlands.
60. Roberts, K.N., et al., *Thermal Behavior of Core-Shell Rubber/Styrene Monomer Gels.* Journal of Polymer Science: Part B: Polymer Physics, 2000. **38**: p. 3136–3150.
61. Vikki, T., et al., *Molecular Recognition Solvents for Electrically Conductive Polyaniline.* Macromolecules, 1996. **29**(8): p. 2945-2953.
62. W. H. Höhne, W. Hemminger, and H.-J. Flammersheim., *Differential scanning calorimetry : an introduction for practitioners* 1996, New York: Springer.
63. Reading, M., A. Luget, and R. Wilson, *Modulated differential scanning calorimetry.* Thermochimica Acta, 1994. **238**(0): p. 295-307.
64. Gill, P., S. Sauerbrunn, and M. Reading, *Modulated differential scanning calorimetry.* Journal of Thermal Analysis and Calorimetry, 1993. **40**(3): p. 931-939.
65. Liu, T., et al., *Nonisothermal melt and cold crystallization kinetics of poly(aryl ether ether ketone ketone).* Polymer Engineering & Science, 1997. **37**(3): p. 568-575.
66. Wu, D., et al., *Nonisothermal cold crystallization behavior and kinetics of polylactide/clay nanocomposites.* Journal of Polymer Science Part B: Polymer Physics, 2007. **45**(9): p. 1100-1113.
67. Marosi, G.J., et al., *Thermal Analysis of Multiphase Polymer Systems*, in *Handbook of Multiphase Polymer Systems*2011, John Wiley & Sons, Ltd. p. 359-385.
68. Baba, M., J.-L. Gardette, and J. Lacoste, *Crosslinking on ageing of elastomers II. Comparison of solvent freezing point depression and conventional crosslinking evaluation.* Polymer Degradation and Stability, 1999. **65**(3): p. 415-420.
69. Honiball, D. and W.J. McGill, *A technique for measuring the crosslink densities in both phases of a vulcanizate blend.* Journal of Polymer Science Part B: Polymer Physics, 1988. **26**(7): p. 1529-1537.

70. Kim, S.J., et al., *Preparation and characterizations of interpenetrating polymer network hydrogels of poly(ethylene oxide) and poly(methyl methacrylate).* Journal of Applied Polymer Science, 2003. **89**(1): p. 258-262.
71. Kim, S.J., C.K. Lee, and S.I. Kim, *Characterization of the water state of hyaluronic acid and poly(vinyl alcohol) interpenetrating polymer networks.* Journal of Applied Polymer Science, 2004. **92**(3): p. 1467-1472.
72. Kim, S.J., S.G. Yoon, and S.I. Kim, *Synthesis and characterization of an interpenetrating polymer network composed of poly(methacrylic acid) and poly(vinyl alcohol).* Polymer International, 2005. **54**(1): p. 149-152.
73. Kim, S.J., S.G. Yoon, and S.I. Kim, *Synthesis and characteristics of interpenetrating polymer network hydrogels composed of alginate and poly(diallydimethylammonium chloride).* Journal of Applied Polymer Science, 2004. **91**(6): p. 3705-3709.
74. Riande, E., et al., *Polymer Viscoelasticity: Stress and Strain in Practice*1999, New York: Marcel Dekker
75. Honiball, D., M.G. Huson, and W.J. McGill, *A nucleation theory for the anomalous freezing point depression of solvents in swollen rubber gels.* Journal of Polymer Science Part B: Polymer Physics, 1988. **26**(12): p. 2413-2431.
76. Laaksonen, T.J. and Y.H. Roos, *Water Sorption and Dielectric Relaxations of Wheat Dough (Containing Sucrose, NaCl, and their Mixtures).* Journal of Cereal Science, 2003. **37**(3): p. 319-326.
77. Y. Vodovotz, L. Hallberg, and P. Chinachoti, *Effect of Aging and Drying on Thermomechanical Properties of White Bread as Characterized by Dynamic Mechanical Analysis (DMA) and Differential Scanning Calorimetry (DSC).* Cereal Chem., 1996. **73**(2): p. 264-270.

Appendix A: Thermal Expansion of the Organogel

Thermal expansion of the 900s cured organogel material was measured by a TA Instruments Q400 Thermo-mechanical analyzer. A quartz macro-expansion probe with a diameter of 6 mm was used for the measurements (Figure A-1).

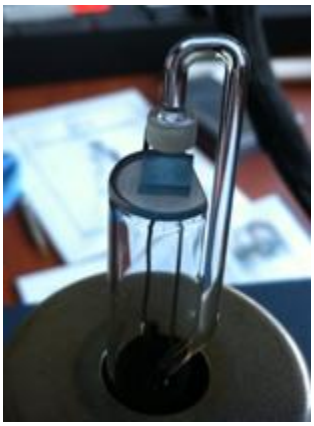

Figure A-1: Macro-expansion probe and the organogel specimen for TMA measurements

Organogel materials were heated at 5°C/min heating rate and the thermal expansion was constantly measured by the instrument. A representative TMA plot is shown in Figure A-2.

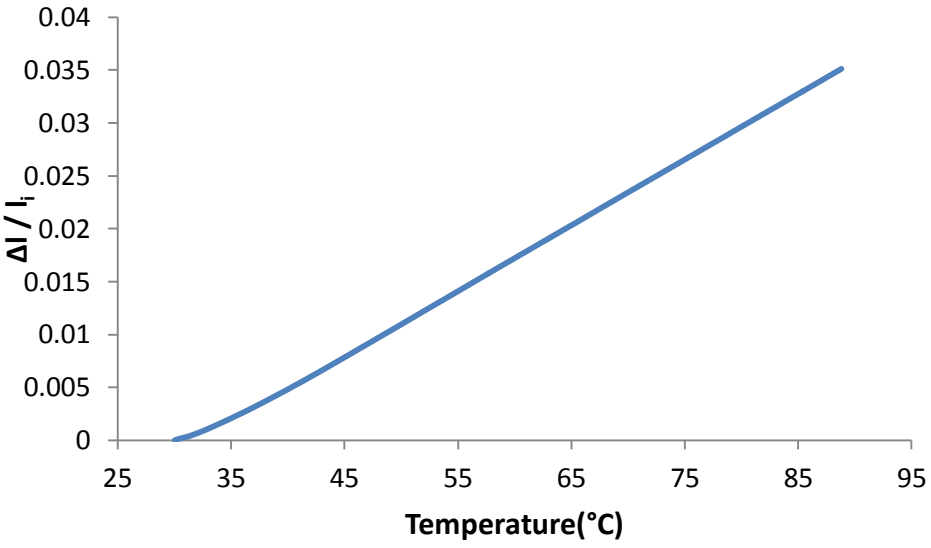

Figure A-2: Thermomechanical analysis plot of 900s cured organogel

From the thermomechanical analysis results, the linear coefficient of thermal expansion of the organogel was found to be 6.29×10^{-4} 1/°C.